

Customizing Text-to-Image Diffusion with Camera Viewpoint Control

Nupur Kumari^{1*} Grace Su^{1*} Richard Zhang²
 Taesung Park² Eli Shechtman² Jun-Yan Zhu¹

¹Carnegie Mellon University ²Adobe Research

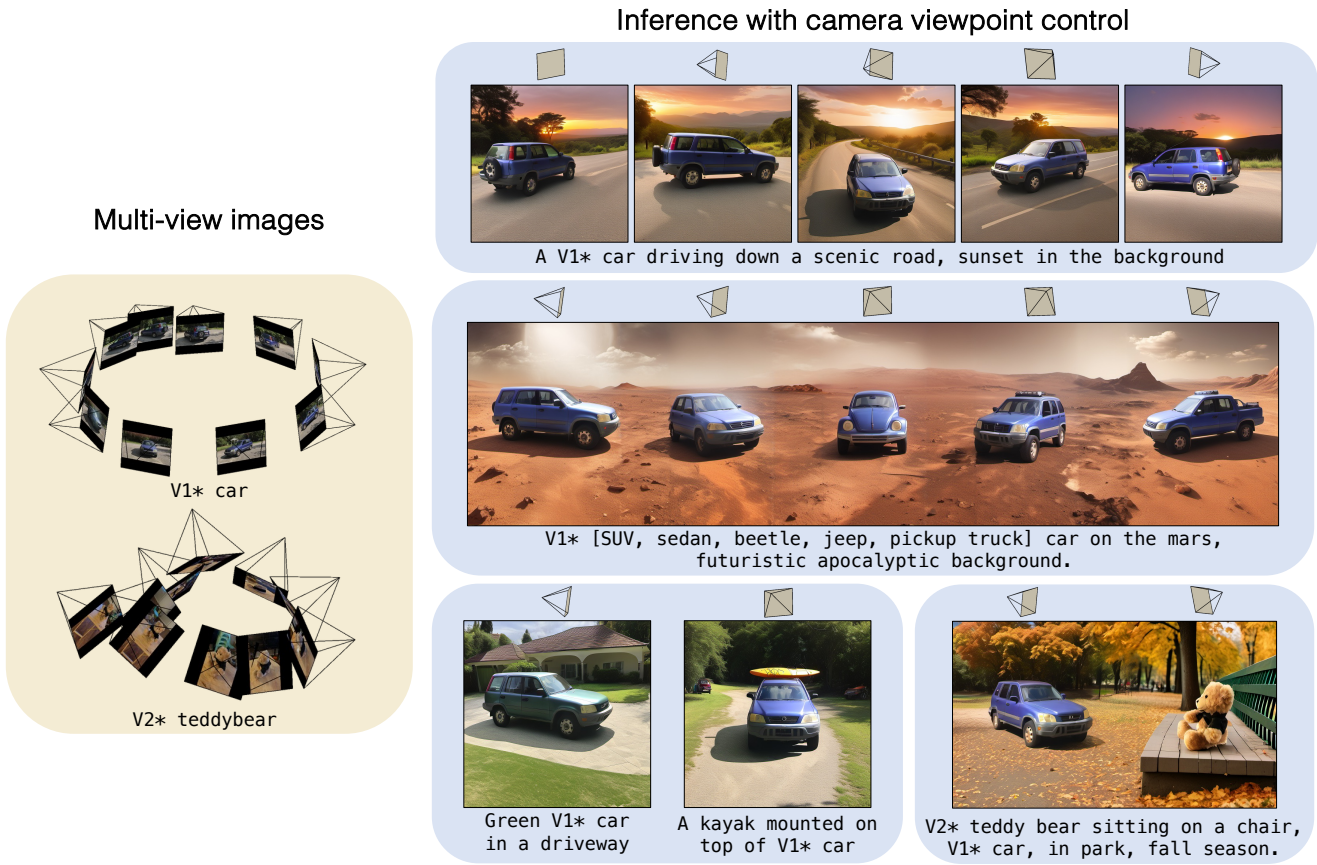


Figure 1. Given multi-view images of a new object (left), we create a customized text-to-image diffusion model with camera pose control. The customized model can synthesize the object (denoted as V^* <category name>) in novel appearances and scenes, such as A green V^* car, or A beetle-like V^* car, while allowing users to specify the target camera pose for the object. We can generate panorama images while controlling the camera pose for each object or compose multiple concepts using MultiDiffusion [3] with our model.

Abstract

Model customization introduces new concepts to existing text-to-image models, enabling the generation of the new concept in novel contexts. However, such methods lack ac-

curate camera view control w.r.t the object, and users must resort to prompt engineering (e.g., adding “top-view”) to achieve coarse view control. In this work, we introduce a new task – enabling explicit control of camera viewpoint for model customization. This allows us to modify object properties amongst various background scenes via text prompts,

* indicates equal contribution

all while incorporating the target camera pose as additional control. This new task presents significant challenges in merging a 3D representation from the multi-view images of the new concept with a general, 2D text-to-image model. To bridge this gap, we propose to condition the 2D diffusion process on rendered, view-dependent features of the new object. During training, we jointly adapt the 2D diffusion modules and 3D feature predictions to reconstruct the object’s appearance and geometry while reducing overfitting to the input multi-view images. Our method outperforms existing image editing and model personalization baselines in preserving the custom object’s identity while following the input text prompt and the object’s camera pose.

1. Introduction

Recently, we have witnessed an explosion of works on customizing text-to-image models [16, 23, 45, 74]. They allow us to quickly acquire visual concepts, such as personal objects and favorite places, and reimagine them with new environments and attributes. For instance, we can customize a model on our Teddy bear and prompt it with “Teddy bear on a bench in the park.” Unfortunately, customization methods lack precise camera pose control, as existing diffusion models are trained purely on 2D images without ground truth camera poses. As a result, users often rely on text prompts such as “front-facing” or “side-facing”, a tedious and unwieldy process to control views.

What if we wish to synthesize a new object, e.g., the Teddy bear in Figure 1, in a different context while controlling its pose? In this work, we introduce a new task: given multi-view images of the object, we customize a text-to-image model while enabling precise control of the new object’s camera pose. During inference, our method offers the flexibility of conditioning the generation process on both a target pose and a text prompt.

Neural rendering methods have allowed us to accurately control the 3D viewpoint of an *existing* scene, given multi-view images [4, 5, 39, 57]. Similarly, we seek to imagine the object from novel viewpoints but in a *new* scene. However, as pre-trained diffusion models, such as Latent Diffusion models [72], are built upon a purely 2D representation, connecting the 3D neural representation of the object to the 2D internal features of the diffusion model remains challenging.

In this work, we propose a new method, CustomDiffusion360, to bridge the gap between 3D neural capture and 2D text-to-image diffusion models by providing additional camera pose control w.r.t. the new custom object in 2D text-to-image models. More concretely, given multi-view images of an object, we learn to predict neural feature fields in the intermediate feature spaces of the diffusion model U-Net. To condition the generation process on a target pose, we render the features of the predicted feature fields and then

fuse them with the target pose’s noisy features. This new conditioning module is added to a subset of transformer layers in the pre-trained diffusion model. We only train the parameters of the new feature prediction module to preserve object identity and increase generalization. All parameters of the pre-trained model remain frozen, thus keeping our method computationally and storage efficient.

We build our method on Stable Diffusion-XL [64] and show results on various object categories, such as cars, chairs, motorcycles, teddy bears, and toys. We compare our method with image editing, model customization, and NeRF editing methods. Our method maintains high alignment with the target object and poses while adhering to the user-provided text prompt. We show that directly integrating the 3D object information into the text-to-image model pipeline provides performance gains relative to existing 2D methods. Our method can also be combined with other algorithms [3, 52] for applications like generating objects in different target camera poses while preserving the background, panorama synthesis, or composing multiple concepts. Our code, results, and data are available on our [webpage](#).

2. Related Works

Text-based image synthesis. Large-scale text-to-image models [22, 34, 69, 77, 99] have become ubiquitous with their capabilities of generating photorealistic images from text prompts. This progress has been driven by the availability of large-scale datasets [80] as well as advancements in model architecture and training objectives [19, 35, 36, 63, 79]. Among them, diffusion models [30, 83, 85] have emerged as a powerful family of models that generate images by gradually denoising Gaussian noise. Their learned priors have been found useful in various applications, such as image editing [29, 52, 102] and 3D creation [47, 65].

Image editing. One crucial application enabled by the above models is image editing based on text instructions [61]. For example, SDEdit [52] exploits the denoising nature of diffusion models, guiding generation in later denoising timesteps using edit instructions while preserving the input image layout. Various works aim to improve upon this by embedding the input image into the model’s latent space [38, 55, 60, 85], while some use cross-attention and self-attention mechanism for realistic and targeted edits [10, 13, 25, 29, 62]. Recently, several methods train conditional diffusion models to follow user edit instructions or spatial controls [9, 102]. However, existing methods primarily focus on changing style and appearance, while our work enables both viewpoint and appearance control.

Model customization. While pre-trained models are trained to generate common objects, users often wish to synthesize images with concepts from their own lives. This has given rise to the emerging technique of model personalization or

customization [23, 45, 74]. These methods aim at embedding a new concept, e.g., pet dog, toy, personal car, person, etc., into the output space of text-to-image models. This enables generating new images of the concept in unseen scenarios using the text prompt, e.g., my car in a field of sunflowers. To achieve this, various works fine-tune a small subset of model parameters [26, 32, 45, 89] and/or optimize text token embeddings [1, 23, 92, 104] on the few images of the new concept with different regularizations [45, 74]. More recently, several encoder-based methods have been proposed that train a model on a vast dataset of concept library [2, 24, 46, 75, 81, 90, 94], enabling faster customization during inference. However, none of the existing works allow controlling the camera pose during inference time. In contrast, given the ease of capturing multi-view images of a new concept, in this work, we ask whether we can augment the capabilities of model customization with additional control of the camera pose.

View synthesis. Novel view synthesis aims to render a scene from unseen camera poses, given multi-view images. Recently, the success of volumetric rendering-based approaches like NeRF [54] have led to numerous follow-up works with better quality [4, 5], faster speed [14, 57], and fewer training views [18, 58, 86, 98]. Recent works learn generative models with large-scale multi-view data to learn generalizable representations for novel view synthesis [11, 49, 50, 78, 95, 106]. While our work draws motivation from this line of research, our goal differs - we aim to enable 3D control in text-to-image personalization, rather than capturing real scenes. Recently, Cheng *et al.* [17] and Höllein *et al.* [31] propose adding camera pose in text-to-image diffusion models, while we focus on model customization.

3D editing. Loosely related to our work, many works have been proposed for inserting and manipulating 3D objects within 2D real photographs, using classic geometry-based approaches [15, 37, 41] or recent generative modeling techniques [53, 96, 103]. Instead of editing a single image, our work aims to “edit” the model weights of a pre-trained 2D diffusion model. Many recent works edit [20, 27] or generate [68, 82, 88] a 3D scene given a text prompt or an image. These methods focus on ensuring the multi-view consistency of the scene. Unlike these, we do not aim to edit a 3D multi-view consistent scene, but instead provide additional camera pose control for the new object when customizing text-to-image models.

3. Method

Given multi-view images of an object, we aim to embed the object in the text-to-image diffusion model. We construct our method in order to allow the generation of new variations of the object through text prompts while providing control of the camera pose of the object. Our approach involves fine-tuning a pre-trained text-to-image diffusion model while

conditioning it on a 3D representation of the object learned in the diffusion model’s feature space. In this section, we briefly overview the diffusion model and then explain our method in detail.

3.1. Diffusion Models

Diffusion models [30, 83] are a class of generative models that sample images by iterative denoising of a random Gaussian distribution. The training of the diffusion model consists of a forward Markov process, where real data \mathbf{x}_0 is gradually transformed to random noise $\mathbf{x}_T \sim \mathcal{N}(\mathbf{0}, \mathbf{I})$ by sequentially adding Gaussian perturbations in T timesteps, i.e., $\mathbf{x}_t = \sqrt{\alpha_t}\mathbf{x}_0 + \sqrt{1 - \alpha_t}\epsilon$. The model is trained to learn the backward process, i.e.,

$$p_\theta(\mathbf{x}_0|\mathbf{c}) = \int \left[p_\theta(\mathbf{x}_T) \prod p_\theta^t(\mathbf{x}_{t-1}|\mathbf{x}_t, \mathbf{c}) \right] d\mathbf{x}_{1:T}, \quad (1)$$

The training objective maximizes the variational lower bound, which can be simplified to a simple reconstruction loss:

$$\mathbb{E}_{\mathbf{x}_t, t, \mathbf{c}, \epsilon \sim \mathcal{N}(\mathbf{0}, \mathbf{I})} [w_t \|\epsilon - \epsilon_\theta(\mathbf{x}_t, t, \mathbf{c})\|], \quad (2)$$

where \mathbf{c} can be any modality to condition the generation process. The model is trained to predict the noise added to create the input noisy image \mathbf{x}_t . During inference, we gradually denoise a random Gaussian noise for a fixed set of timesteps. Various sampling strategies [35, 51, 85] have been proposed to reduce the number of sampling steps T compared to the usual 1000 timesteps in training.

3.2. Customization with Camera Pose Control

Model customization aims to condition the model on a new concept, given N representative images of the concept $\mathcal{Y} = \{\mathbf{y}_i\}_{i=1}^N$, i.e., to model $p(\mathbf{x}|\mathcal{Y}, \mathbf{c})$ with text prompt \mathbf{c} . In contrast, we aim to additionally condition the model on camera pose, allowing more control in the generation process. Thus, given a set of multi-view images $\{\mathbf{y}_i\}_{i=1}^N$ and the corresponding camera poses $\{\pi_i\}_{i=1}^N$, we seek to achieve a customized text-to-image model corresponding to the object, i.e., our goal is to learn the conditional distribution $p(\mathbf{x}|\{(\mathbf{y}_i, \pi_i)\}_{i=1}^N, \mathbf{c}, \phi)$, where \mathbf{c} is text prompt and ϕ is the target camera pose. To achieve this, we fine-tune a pre-trained text-to-image diffusion model, which models $p(\mathbf{x}|\mathbf{c})$, with the additional conditioning of target pose and reference views.

Model architecture. In Figure 2, we show our architecture, with an emphasis on the added pose-conditioned transformer block. To begin, we use the Stable Diffusion-XL (SDXL) [64] as the pre-trained text-to-image diffusion model in our work. It is based on the Latent Diffusion Model (LDM) [72], which is trained in an autoencoder [43] latent space. The diffusion model is a U-Net [73] consisting of encoder, middle, and decoder blocks. Each block consists

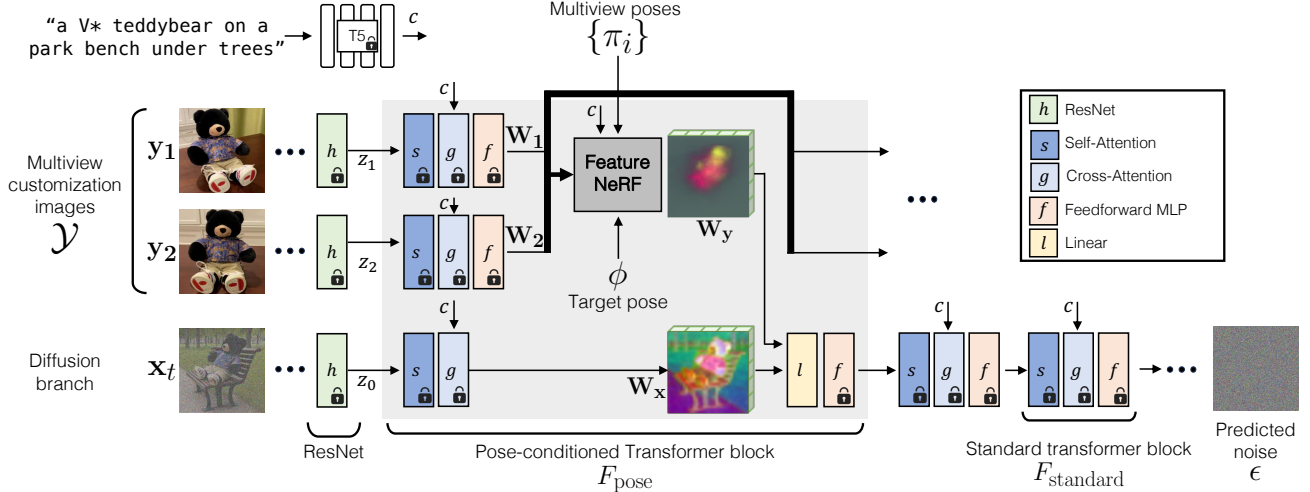


Figure 2. **Overview.** We propose a model customization method that utilizes N reference images defining the 3D structure of an object \mathcal{Y} (we illustrate with 2 views for simplicity). We modify the diffusion model U-Net with pose-conditioned transformer blocks. Our **Pose-conditioned transformer block** features a FeatureNeRF module, which aggregates features from the individual viewpoints to target viewpoint ϕ , as shown in detail in Figure 3. The rendered feature W_y is concatenated with the target noisy feature W_x and projected to the original channel dimension. We use the diffusion U-Net itself to extract features of reference images, as shown in the top row. We only fine-tune the new parameters in linear projection layer l and FeatureNeRF in F_{pose} blocks.

of a ResNet [28], denoted as h , followed by several transformer layers [91]. Each transformer layer consists of a self-attention layer (denoted as s), followed by a cross-attention (denoted as g) with the text condition, and a feed-forward MLP (denoted as f). Given feature map z , output of an intermediate ResNet layer h in the U-Net, a standard transformer block performs $F_{\text{standard}}(z, c) = f(g(s(z), c))$. We modify the transformer layer to incorporate pose conditioning.

Pose-conditioned transformer block. To condition the model on the 3D structure of the object, we modify the transformer block to be a pose-conditioned transformer block $F_{\text{pose}}(z_0, \{z_i, \pi_i\}, c, \phi)$, where z_0 is the feature from the main branch, $\{z_i\}$ are intermediate feature maps corresponding to multi-view images, and $\{\pi_i\}$ and ϕ are reference and target camera poses. To condition on the multi-view images, we learn a radiance field conditioned on reference view features in a feed-forward manner [98]. We extract features $\{W_i \in \mathbb{R}^{H \times W \times C}\}$ from $\{z_i\}$. We use components of pre-trained U-Net itself, F_{standard} , to extract these features and render them into a target pose ϕ using a FeatureNeRF function to obtain 2D feature map W_y .

$$W_i = F_{\text{standard}}(z_i, c), \quad W_y = \text{FeatureNeRF}(\{W_i, \pi_i\}, c, \phi) \quad (3)$$

FeatureNeRF. Here, we describe the aggregation of individual 2D features W_i with 3D poses π_i into a feature map W_y from pose ϕ . Rather than learning NeRF in a feature space [40, 97], our focus is on learning 3D features that the 2D diffusion model can use. From target viewpoint ϕ , for each point \mathbf{p} on a target ray with direction \mathbf{d} , we project the point on the image plane of given views π_i and denote

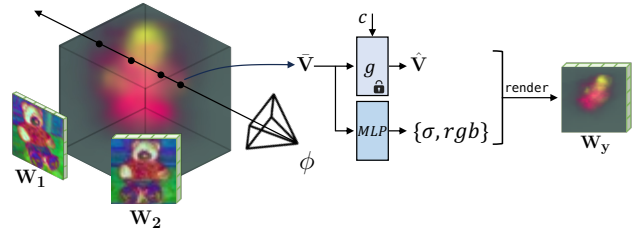


Figure 3. **FeatureNeRF block.** We predict volumetric features $\bar{\mathbf{V}}$ for each 3D point in the grid using reference features $\{W_i\}$ (Eqn. 4). Given this feature, we predict the density σ and color rgb using a 2-layer MLP and use the predicted density to render $\hat{\mathbf{V}}$, which has been updated with text cross-attention g . The predicted rgb is only used to calculate reconstruction loss during training.

projected locations as $\pi_i^{\mathbf{p}}$. We then sample from these coordinates on feature map W_i , predict a feature for the 3D point, and aggregate them with function ψ :

$$\mathbf{V}_i = \text{MLP}(\text{Sample}(W_i; \pi_i^{\mathbf{p}}), \gamma(\mathbf{d}), \gamma(\mathbf{p})), \quad i = 1, \dots, N$$

$$\bar{\mathbf{V}} = \psi(\mathbf{V}_1, \dots, \mathbf{V}_N), \quad (4)$$

where γ is the frequency encoding. We use the weighted average [71] as the aggregation function ψ , where a linear layer predicts the weights based on \mathbf{V}_i, π_i , and target pose ϕ . For each reference view, \mathbf{d} and \mathbf{p} are first transformed in the view coordinate space. We then predict the density and color of the point using a linear layer:

$$(\sigma, \mathbf{C}) = \text{MLP}(\bar{\mathbf{V}}). \quad (5)$$

We also update the aggregated feature with text condition \mathbf{c} using cross-attention:

$$\hat{\mathbf{V}} = \text{CrossAttn}(\bar{\mathbf{V}}, \mathbf{c}), \quad (6)$$

and render this updated intermediate feature using the predicted density σ :

$$\mathbf{W}_y(r) = \sum_{j=1}^{N_f} T_j(1 - \exp(-\sigma_j \delta_j)) \hat{\mathbf{V}}_j, \quad (7)$$

where r is the target ray, $\hat{\mathbf{V}}$ is the aggregated feature of the point in the ray, σ is the predicted density of that point, N_f is the number of sampled points along the ray between the near and far plane of the camera, and $T_j = \exp(-\sum_{k=1}^{j-1} \sigma_k \delta_k)$ handles occlusion until that point.

Conditioning. To process the main target branch, we extract the intermediate 2D feature map after the self s and cross-attention layers g , i.e., $\mathbf{W}_x = g(s(\mathbf{z}_0), \mathbf{c})$. We concatenate \mathbf{W}_x with the rendered features \mathbf{W}_y and then project back into the original feature dimension using a linear layer. Thus, the output of the modified transformer layer is:

$$F_{\text{pose}} = f(l(\mathbf{W}_y \oplus \mathbf{W}_x)), \quad (8)$$

where l is a learnable weight matrix, which projects the feature into the space to be processed by the feedforward layer f . We initialize l such that the contribution from \mathbf{W}_y is zero at the start of training.

Training loss. Our training objective includes learning 3D consistent FeatureNeRF modules, which can contribute to the final goal of reconstructing the target concept in diffusion models output space. Thus, we fine-tune the model using the sum of training losses corresponding to FeatureNeRF and the default diffusion model reconstruction loss:

$$\mathcal{L}_{\text{diffusion}} = \sum_r M w_t \|\epsilon - \epsilon_\theta(\mathbf{x}_t, t, \mathbf{c})\|, \quad (9)$$

where M is the object mask, with the reconstruction loss being calculated only in the object mask region. The losses corresponding to FeatureNeRF consist of RGB reconstruction loss:

$$\mathcal{L}_{\text{rgb}} = \sum_r \|M(r)(\mathbf{C}_{gt}(r) - \sum_{j=1}^{N_f} T_j(1 - \exp(-\sigma_j \delta_j))\mathbf{C})\|, \quad (10)$$

and two mask-based losses – (1) silhouette loss [70] \mathcal{L}_s which forces the rendered opacity to be similar to object mask, and (2) background suppression loss [6, 7] \mathcal{L}_{bg} which enforces the density of all background rays to be zero, as we

only wish to model the object.

$$\mathcal{L}_s = \sum_r \|M(r) - \sum_{j=1}^{N_f} T_j(1 - \exp(-\sigma_j \delta_j))\| \quad (11)$$

$$\mathcal{L}_{\text{bg}} = \sum_r (1 - M(r)) \sum_{j=1}^{N_f} \|(1 - \exp(-\sigma_j \delta_j))\|,$$

Thus, the final training loss is:

$$\mathcal{L} = \mathcal{L}_{\text{diffusion}} + \lambda_{\text{rgb}} \mathcal{L}_{\text{rgb}} + \lambda_{\text{bg}} \mathcal{L}_{\text{bg}} + \lambda_s \mathcal{L}_s, \quad (12)$$

where M is the object mask and λ_i are hyperparameters to control the rendering quality of intermediate images vs the final denoised image. We keep λ_i fixed across all experiments. We assume access to the object’s mask in the image, which is used to calculate the above losses. The three losses corresponding to FeatureNeRF are averaged across all pose-conditioned transformer layers.

Inference. During inference, to balance the text vs. reference view conditions in the final generated image, we combine text and image guidance [9] as shown below:

$$\begin{aligned} \hat{\epsilon}_\theta(\mathbf{x}_t, I = \{\mathbf{y}_i, \pi_i\}_{i=1}^N, \mathbf{c}) &= \epsilon_\theta(\mathbf{x}_t, \emptyset, \emptyset) \\ &+ \lambda_I (\epsilon_\theta(\mathbf{x}_t, I, \emptyset) - \epsilon_\theta(\mathbf{x}_t, \emptyset, \emptyset)) \\ &+ \lambda_c (\epsilon_\theta(\mathbf{x}_t, I, \mathbf{c}) - \epsilon_\theta(\mathbf{x}_t, I, \emptyset)), \end{aligned} \quad (13)$$

where λ_I is the image guidance scale and λ_c is the text guidance scale. Increasing the image guidance scale increases the generated image’s similarity to the reference images. Increasing the text guidance scale increases the generated image’s consistency with the text prompt.

Training details. During training, we sample the N views equidistant from each other and use the first as the target viewpoint and the others as references. We modify 12 transformer layers with pose conditioning out of 70 transformer layers in Stable Diffusion-XL. For rendering, we sample 24 points along the ray. The new concept is described as “V* category”, with V* as a trainable token embedding [23, 45]. Furthermore, to reduce overfitting [74], we use generated images of the same category, such as random car images with ChatGPT-generated captions [12]. These images are randomly sampled 25% of the time during training. We also drop the text prompt with 10% probability to be able to use classifier-free guidance. We provide more implementation details in Appendix C.

4. Experiments

Dataset. For our experiments, we select concepts from the Common Objects in 3D (CO3Dv2) dataset [71], commonly used for novel view synthesis, and NAVI [33]. Specifically, we select four categories with three instances from the CO3Dv2 dataset- car, chair, teddy bear, and motorcycle—as



Figure 4. **Qualitative comparison.** Given a particular target pose, we show the qualitative comparison of our method with (1) Image editing methods *SDEdit*, *InstructPix2Pix*, and *LEDITS++* which edit a NeRF rendered image from the input pose, (2) *ViCA-NeRF*, a 3D editing method that trains a NeRF model for each input prompt, and (3) *LoRA + Camera pose*, our proposed baseline where we concatenate camera pose information to text embeddings during LoRA fine-tuning. Our method performs on par or better in keeping the target identity and poses while incorporating the new text prompt—e.g., putting a picnic table next to the SUV car (1st column)—and following multiple text conditions—e.g., turning the chair red and placing it in a white room (3rd column). V* token is used only in ours and the LoRA + Camera pose method. Ground truth rendering from the given pose is shown as an inset in the first three rows. We show more sample comparisons in Figure 15 of Appendix.

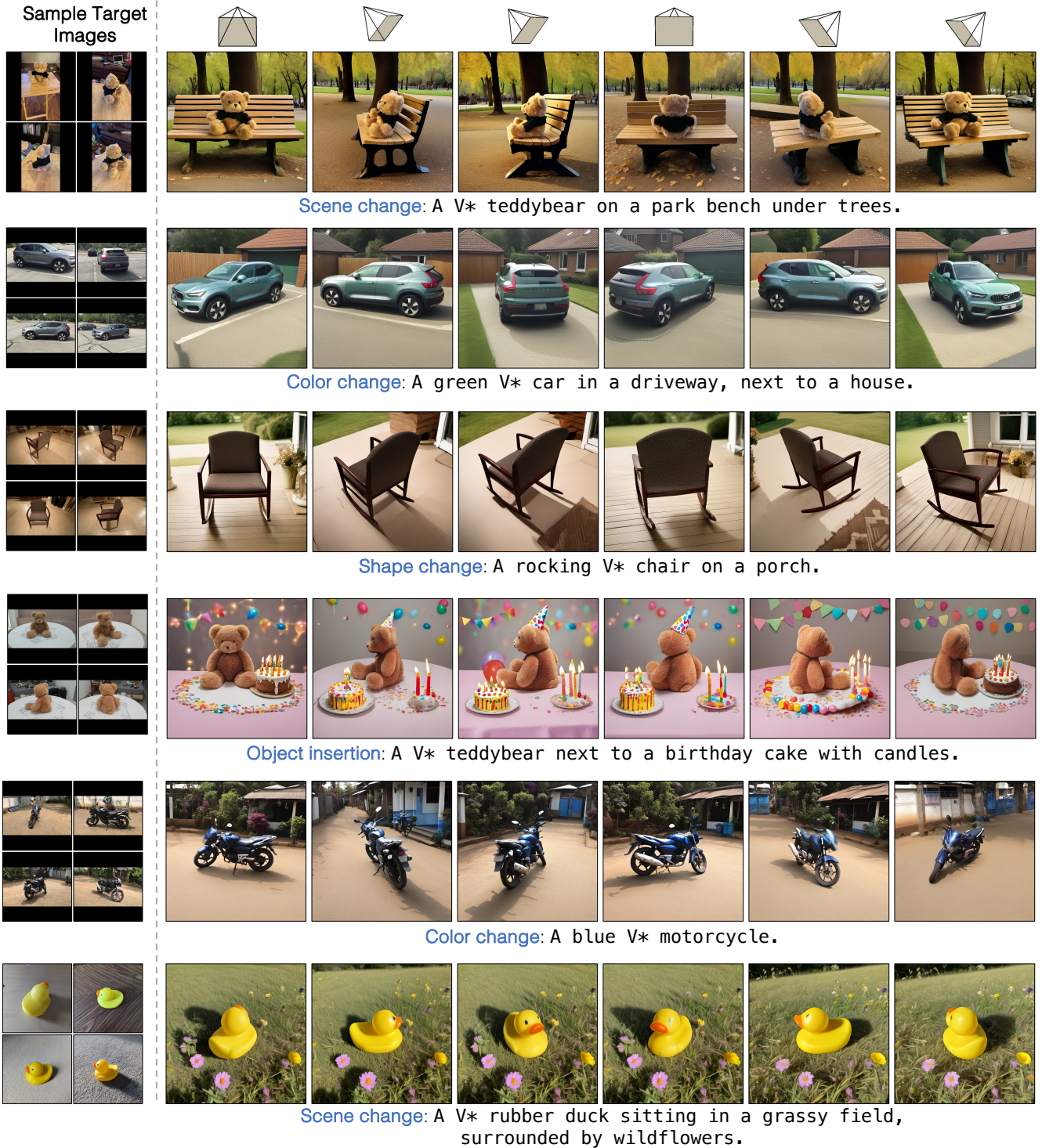


Figure 5. **Qualitative samples with varying pose.** Our method’s results with different text prompts and target poses as conditions. Our method learns the identity of custom objects while allowing the user to control the camera pose and text prompt for generating the object in new contexts, e.g., changing the background scene or object color and shape. In each row, the images were generated with the same seed while changing the camera pose around the object in a turntable manner. Figure 16 in the Appendix shows more such samples. Note that each image in a row is independently generated. We do not aim to generate multi-view consistent scenes.

Method	Text Alignment	Image Alignment	Photorealism
SDEdit	40.06 ± 2.68%	36.08 ± 2.80%	33.11 ± 2.82%
vs. Ours	59.40 ± 2.68%	63.92 ± 2.80%	66.89 ± 3.18%
InstructPix2Pix	44.79 ± 2.58%	29.34 ± 2.24%	27.61 ± 2.63%
vs. Ours	55.21 ± 2.58%	70.66 ± 2.24%	72.39 ± 2.63%
LEDITS++	32.47 ± 2.39%	35.86 ± 2.50%	26.18 ± 2.82%
vs. Ours	67.53 ± 2.39%	64.14 ± 2.50%	73.82 ± 2.82%
Vica-NeRF	27.13 ± 2.83%	24.36 ± 3.35%	12.90 ± 2.67%
vs. Ours	72.87 ± 2.83%	75.64 ± 3.35%	87.10 ± 2.67%
LoRA + Camera pose	32.26 ± 2.67%	66.97 ± 2.50%	52.51 ± 2.75%
vs. Ours	67.64 ± 2.67%	33.03 ± 2.50%	47.49 ± 2.75%

Table 1. **Human preference evaluation.** Our method is preferred over all baselines for text alignment, image alignment to target concept, and photorealism except LoRA + Camera pose, which overfits the training images, as also shown in Figure 4.

Method	Angular error	Camera center error
Ours	14.19	0.080
LoRA + Camera pose	41.14	0.305

Table 2. **Camera pose accuracy** in generated images by ours and the LoRA + Camera pose baseline method. We observe that the baseline usually overfits to training images and does not respect the target pose with new text prompts.

each instance is uniquely identifiable for these categories. From the NAVI dataset, we select two unique toy-like concepts. We use the camera pose provided in the dataset for the multi-view images. A representative image of each concept is shown in Figure 14, Appendix A. For each instance, we sample ~ 100 images and use half for training and half for evaluation. The camera poses are normalized such that the mean of camera location is the origin, and the first camera is at unit norm [100].

Baselines. While no prior method targets our exact task, we use three types of related baselines – (1) 2D image editing methods, which aim to preserve details of the input image and thus keep the object in the same pose as the input image. This includes three recent and publicly available methods: LEDITS++ [8], InstructPix2Pix [9], and SDEdit [52] with Stable Diffusion -1.5 (and SDXL in Appendix A). As image editing methods by themselves do not support camera viewpoint manipulation, we first render a NeRF model [87] in the target pose and then edit the rendered image. (2) Customization-based method, LoRA+Camera pose, where we modify LoRA [32, 76] by concatenating the camera pose information to the text embeddings, following recent work Zero-1-to-3 [49]. (3) VICA-NeRF [20], a 3D editing method that trains a NeRF for each new text prompt. In Appendix C, we provide more details on implementation and hyperparameters for each baseline.

Evaluation metrics. To create an evaluation set, we generate 16 prompts per object category using ChatGPT [12]. We instruct ChatGPT to propose four types of prompts: scene change, color change, object composition, and shape change. We then manually inspect them to remove implausible or

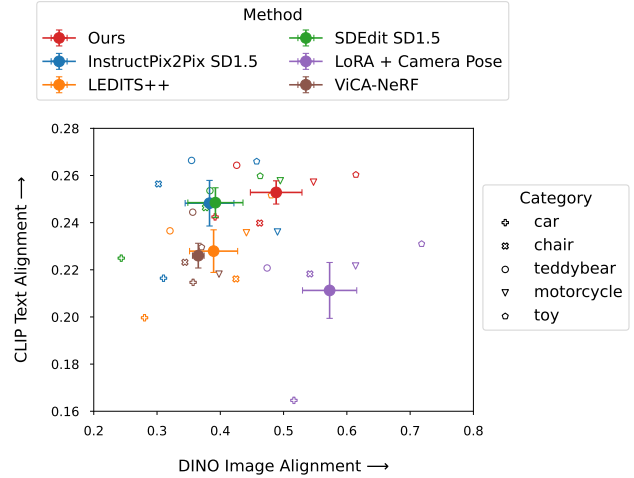


Figure 6. **Quantitative comparison.** We show CLIP scores (higher is better) vs. DINO-v2 scores (higher is better). We plot the performance of each method on each category and the overall mean and standard error (highlighted). Our method results in higher CLIP text alignment while maintaining visual similarity to target concepts, as indicated by DINO-v2 scores. The text alignment of our method compared to SDEdit and InstructPix2Pix is only marginally better as these methods incorporate the text prompt but at the cost of photorealism, as we show in Table 1.

overly complicated text prompts [93]. Table 5 in Appendix B lists all the evaluation prompts.

For a quantitative comparison, we primarily use a pairwise human preference study. We compare our method against each baseline to measure image alignment to target concept, alignment to input text prompt, and photorealism of generated images. In total, we collect ~ 1000 responses per pairwise study using Amazon Mechanical Turk. We also show the performance of our method and baselines on other standard metrics like CLIP Score [67] and DINOv2 [59] image similarity [74] to measure the text- and image-alignment.

To measure whether the object in generated images corresponds to the input camera pose for our method and the LoRA + Camera pose baseline, we use a pretrained model, RayDiffusion [101], to predict the poses from generated images and calculate its error relative to the ground truth camera poses. More details about evaluation are provided in Appendix B.

4.1. Results

Generation quality and adherence. First, we measure the quality of the generation – adherence to the text prompt, the identity preservation to the customized objects, and photorealism – irrespective of the camera pose. For the comparison, we generate 18 images per prompt on 6 target camera poses, totaling 288 images per concept. Table 1 shows the pairwise human preference for our method vs. baselines. Our method is preferred over all baselines except LoRA + Camera pose,

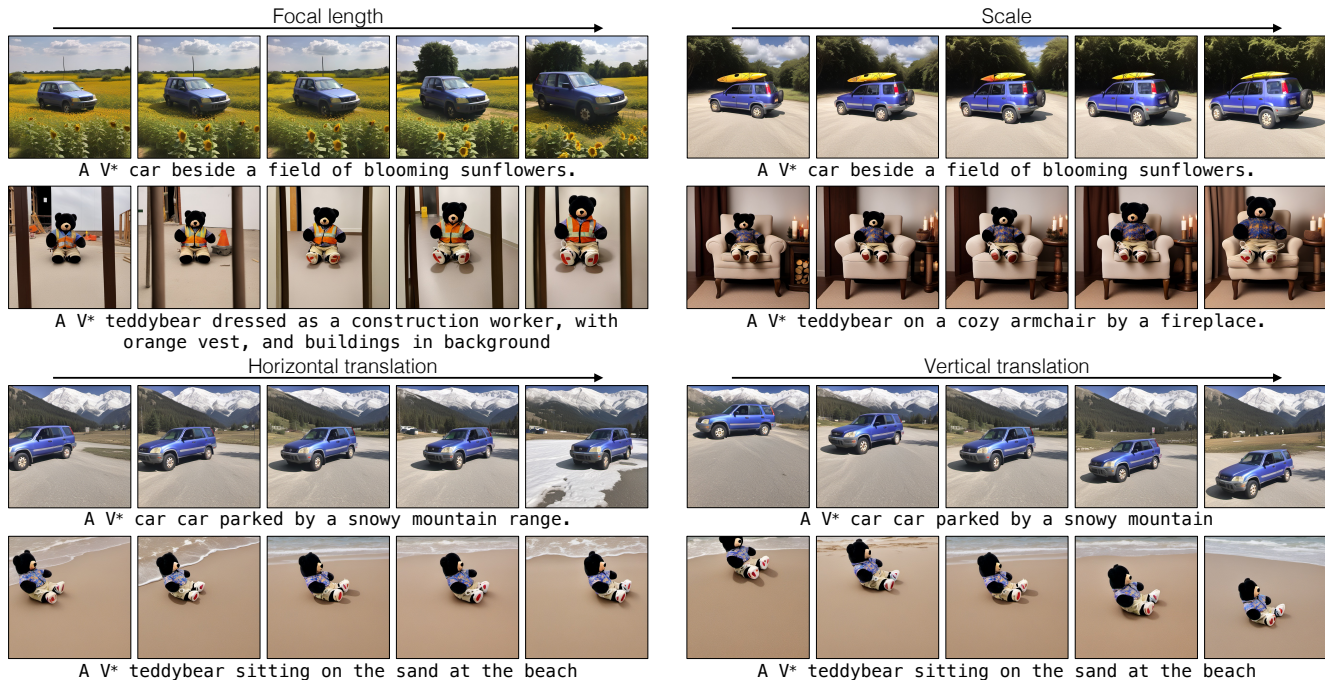


Figure 7. **Extrapolating camera pose from training views.** Our method can generalize to different camera poses, including viewpoints not within the training distribution. *Top left:* We vary the focal length from $\times 0.8$ to $\times 1.4$ of the original focal length. *Top right:* We vary the camera position towards the image plane along the z axis. *Bottom row:* We vary the camera position along the horizontal and vertical axis.

which we observe to overfit on training images. Figure 6 shows the CLIP vs. DINO scores for all methods and object categories. Ideally, a method should have both a high CLIP score and a DINO score, but often, there is a trade-off between text- and image alignment. Our method has on-par or better text alignment relative to the baselines while having better image alignment. We observe that image-editing baselines often require careful hyperparameter tuning for each image. We select the best-performing hyperparameters and keep them fixed across all experiments. We use the ~ 50 validation camera poses not used during training for evaluation and randomly perturb the camera position or focal length. Figure 11 in Appendix B shows sample training and perturbed validation camera poses for the car object.

Camera pose accuracy. Previously, we have measured our method purely on image customization benchmarks. Next, we evaluate the camera pose accuracy as well. Table 2 shows the camera pose accuracy of the generated images in terms of mean angular error and camera center error. We observe that LoRA + Camera pose baseline overfits on training images and can fail at generating images in the correct pose with new text prompts during inference. We evaluate this on validation camera poses of concepts from the CO3Dv2 dataset with the camera’s principal axis pointing towards the object at the scene’s center. This is because RayDiffusion has been trained on this setup of the CO3Dv2 dataset and fails on unique objects.

Qualitative comparison. We show the qualitative comparison of our method with the baselines in Figure 4. As we can see, image-editing-based methods often fail at generating photorealistic results. In the case of LoRA + Camera Pose, we observe that it fails to generalize and overfits to the training views (5th row Figure 4). Finally, the 3D editing-based method Vica-NeRF maintains 3D consistency but generates blurred images for text prompts that change the background scene. Figure 5 shows samples with different text prompts and target camera poses for our method.

Generalization to novel camera poses. Since our method learns a 3D radiance field, we can also extrapolate to unseen camera poses at inference time as shown in Figure 7. We generate images while varying the camera distance from the object (scale), focal length, or camera position along the horizontal and vertical axis.

Applications. Our method can be combined with existing image editing methods as well. Figure 8a shows an example where we use SDEdit [52] to in-paint the object in varying poses while keeping the same background.

We can also generate interesting panoramas using Multi-Diffusion [3], where the object’s placement in each grid is controlled by our method, as shown in Figure 8b. Moreover, since we learn a 3D consistent FeatureNeRF for the new concept, we can compose multiple instances of the object in feature space [84], with each instance in a different camera pose. Figure 8c shows an example of two teddy bears facing

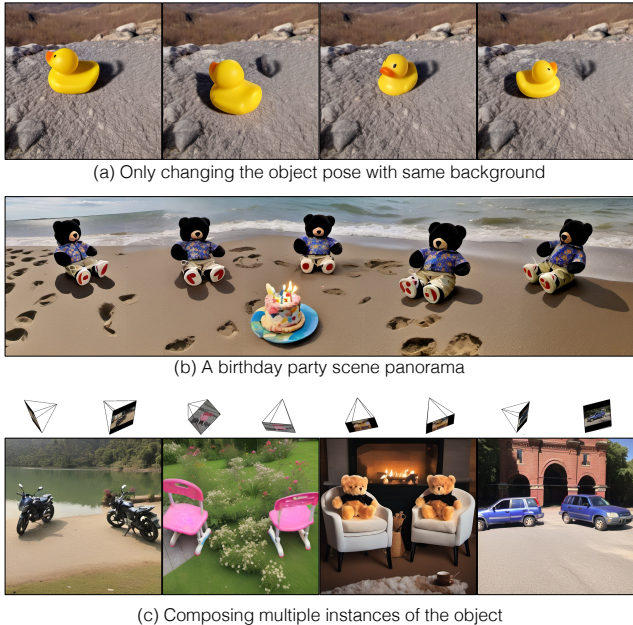


Figure 8. **Applications.** 1st row: Our method can be combined with other image editing methods as well. We use SDEdit with our method to in-paint the rubber duck in different poses while keeping the same background. 2nd row: We can generate interesting panorama shots by controlling the camera pose of the object in each grid independently. 3rd row: We can also compose the radiance field predicted by FeatureNeRF to control the relative pose while generating multiple instances of the object.

Method	Text Align.	Image Align.		Camera-pose Accuracy	
	CLIP-score \uparrow	fore-ground \uparrow	back-ground \downarrow	Angular error \downarrow	Camera center error \downarrow
Ours	0.248	0.471	0.348	14.19	0.080
w/o Eqn. 6	0.250	0.460	0.340	16.08	0.096
w/o $\mathcal{L}_{bg} + \mathcal{L}_s$	0.239	0.471	0.371	11.83	0.068

Table 3. **Ablation experiments.** Not enriching volumetric features with text cross-attention (Eqn. 6) has an adverse effect on image alignment. Not having mask-based losses (Eqn. 11) leads to overfitting on training images and decreases the text alignment. The worst performing metrics are grayed. Our final method achieves a balance between the input conditions of the target concept, text prompt, and camera pose.

each other sitting on the armchair. Here, we additionally use DenseDiffusion [42] to modulate the attention maps and guide the generation of each object instance to only appear in the corresponding region predicted by FeatureNeRF. At the same time, the attention maps of the empty region predicted by FeatureNeRF are modulated to match the part of the text prompt describing the image’s background.

4.2. Ablation

In this section, we perform ablation experiments regarding different components of our method and show its contribution. All ablation studies are done on CO3D-v2 instances

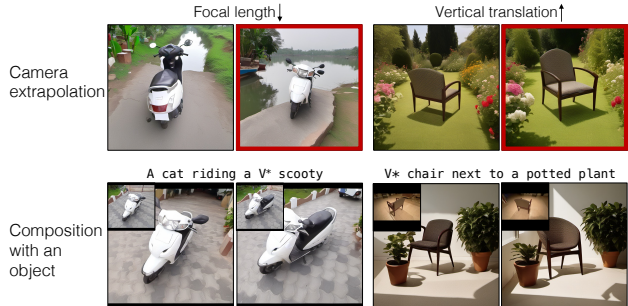


Figure 9. **Limitations.** Our method can fail when extrapolating camera poses far from the training image camera poses, e.g., changing focal length (top left) or translating camera s.t. the object is not in the center (top right) as the pre-trained model is often biased towards generating the object in the center. Also, it can fail to follow the input text prompt or the exact camera pose when multiple objects are composed in a scene (bottom row).

with validation camera poses.

Background losses. When removing the silhouette and background loss, as explained in Eqn. 11 from training, we observe a decrease in text alignment and overfitting on training images as shown in Table 3. Figure 12 in Appendix A shows qualitatively that the model generates images with backgrounds more similar to the training views. This is also reflected by the higher similarity between generated images and background regions of the training images (3rd column Table 3) compared to our final method.

Text cross-attention in FeatureNeRF. We also enrich the 3D learned features with text cross-attention as shown in Eqn. 6. We perform the ablation experiment of removing this component from the module. Table 3 shows that this leads to a drop in image alignment with the target concept. Thus, cross-attention with text in the volumetric feature space helps the module learn the target concept better.

5. Discussion and Limitations

We introduce a new task of customizing text-to-image models with camera viewpoint control. Our method jointly learns 3D feature prediction modules and adapts 2D diffusion attention modules to be conditioned on these features. This enables synthesizing the object with new text prompts and precise object pose control. While our method outperforms existing image editing and model customization approaches, it still has several limitations, as we discuss below.

Limitations. As we show in Figure 9, our method struggles at generalizing to extreme camera poses that were not seen during training and resorts to either changing the object identity or generating the object in a seen pose. We expect this to improve by adding more camera pose variations during training. An additional case when our method struggles to follow the camera pose is when the text prompt adds multiple new objects. We hypothesize that in such challenging sce-

narios, the model is biased towards generating front views, often seen in training. Also, our proposed pose-conditioning module is trained with a finetuning-based method. Exploring pose-conditioning in a zero-shot customization and editing methods [16, 24] may help reduce the time and computation as well. Here, we focus on enabling camera view control while generating rigid objects. Future work includes extending this conditioning to handle dynamic objects that change the pose in between reference views. One potential way to address this is using a representation based on dynamic and non-rigid NeRF methods [21, 66, 84].

Acknowledgment. We are thankful to Kangle Deng, Sheng-Yu Wang, and Gaurav Parmar for their helpful comments and discussion and to Sean Liu, Ruihan Gao, Yufei Ye, and Bharath Raj for proofreading the draft. This work was partly done by Nupur Kumari during the Adobe internship. The work is partly supported by Adobe Research, the Packard Fellowship, the Amazon Faculty Research Award, and NSF IIS-2239076. Grace Su is supported by the NSF Graduate Research Fellowship (Grant No. DGE2140739).

References

- [1] Yuval Alaluf, Elad Richardson, Gal Metzer, and Daniel Cohen-Or. A neural space-time representation for text-to-image personalization. *ACM Transactions on Graphics (TOG)*, 2023. 3
- [2] Moab Arar, Rinon Gal, Yuval Atzmon, Gal Chechik, Daniel Cohen-Or, Ariel Shamir, and Amit H. Bermano. Domain-agnostic tuning-encoder for fast personalization of text-to-image models. In *SIGGRAPH Asia 2023 Conference Papers*, 2023. 3
- [3] Omer Bar-Tal, Lior Yariv, Yaron Lipman, and Tali Dekel. Multidiffusion: Fusing diffusion paths for controlled image generation. In *International Conference on Machine Learning (ICML)*, 2023. 1, 2, 9
- [4] Jonathan T Barron, Ben Mildenhall, Matthew Tancik, Peter Hedman, Ricardo Martin-Brualla, and Pratul P Srinivasan. Mip-nerf: A multiscale representation for anti-aliasing neural radiance fields. In *IEEE International Conference on Computer Vision (ICCV)*, 2021. 2, 3
- [5] Jonathan T Barron, Ben Mildenhall, Dor Verbin, Pratul P Srinivasan, and Peter Hedman. Zip-nerf: Anti-aliased grid-based neural radiance fields. In *IEEE International Conference on Computer Vision (ICCV)*, 2023. 2, 3
- [6] Mark Boss, Raphael Braun, Varun Jampani, Jonathan T Barron, Ce Liu, and Hendrik Lensch. Nerf: Neural reflectance decomposition from image collections. In *IEEE International Conference on Computer Vision (ICCV)*, 2021. 5
- [7] Mark Boss, Andreas Engelhardt, Abhishek Kar, Yuanzhen Li, Deqing Sun, Jonathan Barron, Hendrik Lensch, and Varun Jampani. Samurai: Shape and material from unconstrained real-world arbitrary image collections. In *Conference on Neural Information Processing Systems (NeurIPS)*, 2022. 5
- [8] Manuel Brack, Felix Friedrich, Katharina Kornmeier, Linoy Tsaban, Patrick Schramowski, Kristian Kersting, and Apolinário Passos. Ledits++: Limitless image editing using text-to-image models. *arXiv preprint arXiv:2311.16711*, 2023. 8, 16, 17
- [9] Tim Brooks, Aleksander Holynski, and Alexei A Efros. Instructpix2pix: Learning to follow image editing instructions. In *IEEE Conference on Computer Vision and Pattern Recognition (CVPR)*, 2023. 2, 5, 8, 17
- [10] Mingdeng Cao, Xintao Wang, Zhongang Qi, Ying Shan, Xiaohu Qie, and Yinqiang Zheng. Masactrl: Tuning-free mutual self-attention control for consistent image synthesis and editing. In *IEEE International Conference on Computer Vision (ICCV)*, 2023. 2
- [11] Eric R Chan, Koki Nagano, Matthew A Chan, Alexander W Bergman, Jeong Joon Park, Axel Levy, Miika Aittala, Shalini De Mello, Tero Karras, and Gordon Wetzstein. Genvs: Generative novel view synthesis with 3d-aware diffusion models. In *IEEE International Conference on Computer Vision (ICCV)*, 2023. 3
- [12] ChatGPT. Chatgpt. <https://chat.openai.com/chat>, 2022. 5, 8
- [13] Hila Chefer, Yuval Alaluf, Yael Vinker, Lior Wolf, and Daniel Cohen-Or. Attend-and-excite: Attention-based semantic guidance for text-to-image diffusion models. *ACM Transactions on Graphics (TOG)*, 2023. 2
- [14] Anpei Chen, Zexiang Xu, Andreas Geiger, Jingyi Yu, and Hao Su. Tensorf: Tensorial radiance fields. In *European Conference on Computer Vision (ECCV)*, 2022. 3
- [15] Tao Chen, Zhe Zhu, Ariel Shamir, Shi-Min Hu, and Daniel Cohen-Or. 3-sweep: Extracting editable objects from a single photo. *ACM Transactions on graphics (TOG)*, 2013. 3
- [16] Wenhui Chen, Hexiang Hu, Yandong Li, Nataniel Rui, Xuhui Jia, Ming-Wei Chang, and William W Cohen. Subject-driven text-to-image generation via apprenticeship learning. In *Conference on Neural Information Processing Systems (NeurIPS)*, 2023. 2, 11
- [17] Ta-Ying Cheng, Matheus Gadelha, Thibault Groueix, Matthew Fisher, Radomir Mech, Andrew Markham, and Niki Trigoni. Learning continuous 3d words for text-to-image generation. In *IEEE Conference on Computer Vision and Pattern Recognition (CVPR)*, 2024. 3
- [18] Kangle Deng, Andrew Liu, Jun-Yan Zhu, and Deva Ramanan. Depth-supervised nerf: Fewer views and faster training for free. In *IEEE Conference on Computer Vision and Pattern Recognition (CVPR)*, 2022. 3
- [19] Prafulla Dhariwal and Alexander Nichol. Diffusion models beat gans on image synthesis. In *Conference on Neural Information Processing Systems (NeurIPS)*, 2021. 2
- [20] Jiahua Dong and Yu-Xiong Wang. Vica-nerf: View-consistency-aware 3d editing of neural radiance fields. In *Conference on Neural Information Processing Systems (NeurIPS)*, 2023. 3, 8, 17
- [21] Sara Fridovich-Keil, Giacomo Meanti, Frederik Rahbæk Warburg, Benjamin Recht, and Angjoo Kanazawa. K-planes: Explicit radiance fields in space, time, and appearance. In *IEEE Conference on Computer Vision and Pattern Recognition (CVPR)*, 2023. 11

- [22] Oran Gafni, Adam Polyak, Oron Ashual, Shelly Sheynin, Devi Parikh, and Yaniv Taigman. Make-a-scene: Scene-based text-to-image generation with human priors. In *European Conference on Computer Vision (ECCV)*, 2022. [2](#)
- [23] Rinon Gal, Yuval Alaluf, Yuval Atzmon, Or Patashnik, Amit H Bermano, Gal Chechik, and Daniel Cohen-Or. An image is worth one word: Personalizing text-to-image generation using textual inversion. In *International Conference on Learning Representations (ICLR)*, 2023. [2](#), [3](#), [5](#)
- [24] Rinon Gal, Moab Arar, Yuval Atzmon, Amit H Bermano, Gal Chechik, and Daniel Cohen-Or. Encoder-based domain tuning for fast personalization of text-to-image models. *ACM Transactions on Graphics (TOG)*, 2023. [3](#), [11](#)
- [25] Songwei Ge, Taesung Park, Jun-Yan Zhu, and Jia-Bin Huang. Expressive text-to-image generation with rich text. In *IEEE International Conference on Computer Vision (ICCV)*, 2023. [2](#)
- [26] Ligong Han, Yinxiao Li, Han Zhang, Peyman Milanfar, Dimitris Metaxas, and Feng Yang. Svdiff: Compact parameter space for diffusion fine-tuning. In *IEEE International Conference on Computer Vision (ICCV)*, 2023. [3](#)
- [27] Ayaan Haque, Matthew Tancik, Alexei A Efros, Aleksander Holynski, and Angjoo Kanazawa. Instruct-nerf2nerf: Editing 3d scenes with instructions. In *IEEE International Conference on Computer Vision (ICCV)*, 2023. [3](#), [17](#)
- [28] Kaiming He, Xiangyu Zhang, Shaoqing Ren, and Jian Sun. Deep residual learning for image recognition. In *IEEE Conference on Computer Vision and Pattern Recognition (CVPR)*, 2016. [4](#)
- [29] Amir Hertz, Ron Mokady, Jay Tenenbaum, Kfir Aberman, Yael Pritch, and Daniel Cohen-Or. Prompt-to-prompt image editing with cross attention control. In *International Conference on Learning Representations (ICLR)*, 2023. [2](#)
- [30] Jonathan Ho, Ajay Jain, and Pieter Abbeel. Denoising diffusion probabilistic models. In *Conference on Neural Information Processing Systems (NeurIPS)*, 2020. [2](#), [3](#)
- [31] Lukas Höllein, Aljazz Bovzirc, Norman Müller, David Novotny, Hung-Yu Tseng, Christian Richardt, Michael Zollhöfer, and Matthias Nießner. Viewdiff: 3d-consistent image generation with text-to-image models. In *IEEE Conference on Computer Vision and Pattern Recognition (CVPR)*, 2024. [3](#)
- [32] Edward J Hu, Yelong Shen, Phillip Wallis, Zeyuan Allen-Zhu, Yuanzhi Li, Shean Wang, Lu Wang, and Weizhu Chen. Lora: Low-rank adaptation of large language models. In *International Conference on Learning Representations (ICLR)*, 2022. [3](#), [8](#), [16](#), [18](#)
- [33] Varun Jampani, Kevis-Kokitsi Maninis, Andreas Engelhardt, Arjun Karapur, Karen Truong, Kyle Sargent, Stefan Popov, André Araujo, Ricardo Martin Brualla, Kaushal Patel, et al. Navi: Category-agnostic image collections with high-quality 3d shape and pose annotations. In *Conference on Neural Information Processing Systems (NeurIPS)*, 2023. [5](#)
- [34] Minguk Kang, Jun-Yan Zhu, Richard Zhang, Jaesik Park, Eli Shechtman, Sylvain Paris, and Taesung Park. Scaling up gans for text-to-image synthesis. In *IEEE Conference on Computer Vision and Pattern Recognition (CVPR)*, 2023. [2](#)
- [35] Tero Karras, Miika Aittala, Timo Aila, and Samuli Laine. Elucidating the design space of diffusion-based generative models. In *Conference on Neural Information Processing Systems (NeurIPS)*, 2022. [2](#), [3](#), [17](#)
- [36] Tero Karras, Miika Aittala, Jaakko Lehtinen, Janne Hellsten, Timo Aila, and Samuli Laine. Analyzing and improving the training dynamics of diffusion models. *arXiv preprint arXiv:2312.02696*, 2023. [2](#)
- [37] Kevin Karsch, Varsha Hedau, David Forsyth, and Derek Hoiem. Rendering synthetic objects into legacy photographs. *ACM Transactions on graphics (TOG)*, 2011. [3](#)
- [38] Bahjat Kwar, Shiran Zada, Oran Lang, Omer Tov, Huiwen Chang, Tali Dekel, Inbar Mosseri, and Michal Irani. Imagic: Text-based real image editing with diffusion models. In *IEEE Conference on Computer Vision and Pattern Recognition (CVPR)*, 2023. [2](#)
- [39] Bernhard Kerbl, Georgios Kopanas, Thomas Leimkühler, and George Drettakis. 3d gaussian splatting for real-time radiance field rendering. *ACM Transactions on Graphics*, 42(4), 2023. [2](#)
- [40] Justin Kerr, Chung Min Kim, Ken Goldberg, Angjoo Kanazawa, and Matthew Tancik. Lorf: Language embedded radiance fields. In *IEEE International Conference on Computer Vision (ICCV)*, 2023. [4](#)
- [41] Natasha Kholgade, Tomas Simon, Alexei Efros, and Yaser Sheikh. 3d object manipulation in a single photograph using stock 3d models. *ACM Transactions on graphics (TOG)*, 2014. [3](#)
- [42] Yunji Kim, Jiyoung Lee, Jin-Hwa Kim, Jung-Woo Ha, and Jun-Yan Zhu. Dense text-to-image generation with attention modulation. In *IEEE International Conference on Computer Vision (ICCV)*, 2023. [10](#)
- [43] Diederik P Kingma and Max Welling. Auto-encoding variational bayes. In *International Conference on Learning Representations (ICLR)*, 2014. [3](#)
- [44] Alexander Kirillov, Eric Mintun, Nikhila Ravi, Hanzi Mao, Chloe Rolland, Laura Gustafson, Tete Xiao, Spencer Whitehead, Alexander C Berg, Wan-Yen Lo, et al. Segment anything. In *IEEE International Conference on Computer Vision (ICCV)*, 2023. [16](#)
- [45] Nupur Kumari, Bingliang Zhang, Richard Zhang, Eli Shechtman, and Jun-Yan Zhu. Multi-concept customization of text-to-image diffusion. In *IEEE Conference on Computer Vision and Pattern Recognition (CVPR)*, 2023. [2](#), [3](#), [5](#)
- [46] Dongxu Li, Junnan Li, and Steven CH Hoi. Blip-diffusion: Pre-trained subject representation for controllable text-to-image generation and editing. In *Conference on Neural Information Processing Systems (NeurIPS)*, 2023. [3](#), [17](#)
- [47] Chen-Hsuan Lin, Jun Gao, Luming Tang, Towaki Takikawa, Xiaohui Zeng, Xun Huang, Karsten Kreis, Sanja Fidler, Ming-Yu Liu, and Tsung-Yi Lin. Magic3d: High-resolution text-to-3d content creation. In *IEEE Conference on Computer Vision and Pattern Recognition (CVPR)*, 2023. [2](#)
- [48] Luping Liu, Yi Ren, Zhijie Lin, and Zhou Zhao. Pseudo numerical methods for diffusion models on manifolds. In *International Conference on Learning Representations (ICLR)*, 2022. [17](#)

- [49] Ruoshi Liu, Rundi Wu, Basile Van Hoorick, Pavel Tokmakov, Sergey Zakharov, and Carl Vondrick. Zero-1-to-3: Zero-shot one image to 3d object. In *IEEE International Conference on Computer Vision (ICCV)*, 2023. 3, 8
- [50] Yuan Liu, Cheng Lin, Zijiao Zeng, Xiaoxiao Long, Lingjie Liu, Taku Komura, and Wenping Wang. Syncdreamer: Generating multiview-consistent images from a single-view image. In *International Conference on Learning Representations (ICLR)*, 2024. 3
- [51] Cheng Lu, Yuhao Zhou, Fan Bao, Jianfei Chen, Chongxuan Li, and Jun Zhu. Dpm-solver: A fast ode solver for diffusion probabilistic model sampling in around 10 steps. In *Conference on Neural Information Processing Systems (NeurIPS)*, 2022. 3
- [52] Chenlin Meng, Yutong He, Yang Song, Jiaming Song, Jiajun Wu, Jun-Yan Zhu, and Stefano Ermon. Sdedit: Guided image synthesis and editing with stochastic differential equations. In *International Conference on Learning Representations (ICLR)*, 2022. 2, 8, 9, 17
- [53] Oscar Michel, Anand Bhattad, Eli VanderBilt, Ranjay Krishna, Aniruddha Kembhavi, and Tanmay Gupta. Object 3dit: Language-guided 3d-aware image editing. In *Conference on Neural Information Processing Systems (NeurIPS)*, 2023. 3
- [54] Ben Mildenhall, Pratul P Srinivasan, Matthew Tancik, Jonathan T Barron, Ravi Ramamoorthi, and Ren Ng. Nerf: Representing scenes as neural radiance fields for view synthesis. *Communications of the ACM*, 2021. 3
- [55] Ron Mokady, Amir Hertz, Kfir Aberman, Yael Pritch, and Daniel Cohen-Or. Null-text inversion for editing real images using guided diffusion models. In *IEEE Conference on Computer Vision and Pattern Recognition (CVPR)*, 2023. 2
- [56] Chong Mou, Xintao Wang, Liangbin Xie, Yanze Wu, Jian Zhang, Zhongang Qi, and Ying Shan. T2i-adapter: Learning adapters to dig out more controllable ability for text-to-image diffusion models. In *Conference on Artificial Intelligence (AAAI)*, 2024. 17
- [57] Thomas Müller, Alex Evans, Christoph Schied, and Alexander Keller. Instant neural graphics primitives with a multiresolution hash encoding. *ACM Transactions on Graphics (ToG)*, 2022. 2, 3
- [58] Michael Niemeyer, Jonathan T. Barron, Ben Mildenhall, Mehdi S. M. Sajjadi, Andreas Geiger, and Noha Radwan. Regnerf: Regularizing neural radiance fields for view synthesis from sparse inputs. In *IEEE Conference on Computer Vision and Pattern Recognition (CVPR)*, 2022. 3
- [59] Maxime Oquab, Timothée Darcet, Théo Moutakanni, Huy Vo, Marc Szafraniec, Vasil Khalidov, Pierre Fernandez, Daniel Haziza, Francisco Massa, Alaaeldin El-Nouby, et al. Dinov2: Learning robust visual features without supervision. In *TMLR*, 2023. 8, 16
- [60] Gaurav Parmar, Krishna Kumar Singh, Richard Zhang, Yijun Li, Jingwan Lu, and Jun-Yan Zhu. Zero-shot image-to-image translation. In *ACM SIGGRAPH 2023 Conference Proceedings*, pages 1–11, 2023. 2
- [61] Or Patashnik, Zongze Wu, Eli Shechtman, Daniel Cohen-Or, and Dani Lischinski. Styleclip: Text-driven manipulation of stylegan imagery. In *IEEE International Conference on Computer Vision (ICCV)*, 2021. 2
- [62] Or Patashnik, Daniel Garibi, Idan Azuri, Hadar Averbuch-Elor, and Daniel Cohen-Or. Localizing object-level shape variations with text-to-image diffusion models. In *IEEE International Conference on Computer Vision (ICCV)*, 2023. 2
- [63] William Peebles and Saining Xie. Scalable diffusion models with transformers. In *IEEE International Conference on Computer Vision (ICCV)*, 2023. 2
- [64] Dustin Podell, Zion English, Kyle Lacey, Andreas Blattmann, Tim Dockhorn, Jonas Müller, Joe Penna, and Robin Rombach. Sdxl: Improving latent diffusion models for high-resolution image synthesis. *arXiv preprint arXiv:2307.01952*, 2023. 2, 3, 17
- [65] Ben Poole, Ajay Jain, Jonathan T Barron, and Ben Mildenhall. Dreamfusion: Text-to-3d using 2d diffusion. In *International Conference on Learning Representations (ICLR)*, 2023. 2
- [66] Albert Pumarola, Enric Corona, Gerard Pons-Moll, and Francesc Moreno-Noguer. D-NeRF: Neural Radiance Fields for Dynamic Scenes. In *IEEE Conference on Computer Vision and Pattern Recognition (CVPR)*, 2021. 11
- [67] Alec Radford, Jong Wook Kim, Chris Hallacy, Aditya Ramesh, Gabriel Goh, Sandhini Agarwal, Girish Sastry, Amanda Askell, Pamela Mishkin, Jack Clark, et al. Learning transferable visual models from natural language supervision. In *International Conference on Machine Learning (ICML)*, 2021. 8
- [68] Amit Raj, Srinivas Kaza, Ben Poole, Michael Niemeyer, Nataniel Ruiz, Ben Mildenhall, Shiran Zada, Kfir Aberman, Michael Rubinstein, Jonathan Barron, et al. Dreambooth3d: Subject-driven text-to-3d generation. In *IEEE International Conference on Computer Vision (ICCV)*, 2023. 3
- [69] Aditya Ramesh, Prafulla Dhariwal, Alex Nichol, Casey Chu, and Mark Chen. Hierarchical text-conditional image generation with clip latents. *arXiv preprint arXiv:2204.06125*, 2022. 2
- [70] Nikhila Ravi, Jeremy Reizenstein, David Novotny, Taylor Gordon, Wan-Yen Lo, Justin Johnson, and Georgia Gkioxari. Accelerating 3d deep learning with pytorch3d. *arXiv preprint arXiv:2007.08501*, 2020. 5
- [71] Jeremy Reizenstein, Roman Shapovalov, Philipp Henzler, Luca Sbordone, Devi Labatut, Patrikh, Yanivck Taigman, and David Novotny. Common objects in 3d: Large-scale learning and evaluation of real-life 3d category reconstruction. In *IEEE International Conference on Computer Vision (ICCV)*, 2021. 4, 5
- [72] Robin Rombach, Andreas Blattmann, Dominik Lorenz, Patrick Esser, and Björn Ommer. High-resolution image synthesis with latent diffusion models. In *IEEE Conference on Computer Vision and Pattern Recognition (CVPR)*, 2022. 2, 3
- [73] Olaf Ronneberger, Philipp Fischer, and Thomas Brox. U-net: Convolutional networks for biomedical image segmentation. In *International Conference on Medical image computing and computer-assisted intervention*, 2015. 3

- [74] Nataniel Ruiz, Yuanzhen Li, Varun Jampani, Yael Pritch, Michael Rubinstein, and Kfir Aberman. Dreambooth: Fine tuning text-to-image diffusion models for subject-driven generation. In *IEEE Conference on Computer Vision and Pattern Recognition (CVPR)*, 2023. 2, 3, 5, 8
- [75] Nataniel Ruiz, Yuanzhen Li, Varun Jampani, Wei Wei, Tingbo Hou, Yael Pritch, Neal Wadhwa, Michael Rubinstein, and Kfir Aberman. Hyperdreambooth: Hypernetworks for fast personalization of text-to-image models. *arXiv preprint arXiv:2307.06949*, 2023. 3
- [76] Simo Ryu. Lora-stable diffusion. <https://github.com/cloneofsimon/lora>, 2023. 8, 16
- [77] Chitwan Saharia, William Chan, Saurabh Saxena, Lala Li, Jay Whang, Emily Denton, Seyed Kamyar Seyed Ghasemipour, Burcu Karagol Ayan, S Sara Mahdavi, Rapha Gontijo Lopes, et al. Photorealistic text-to-image diffusion models with deep language understanding. In *Conference on Neural Information Processing Systems (NeurIPS)*, 2022. 2
- [78] Kyle Sargent, Zizhang Li, Tanmay Shah, Charles Herrmann, Hong-Xing Yu, Yunzhi Zhang, Eric Ryan Chan, Dmitry Lagun, Li Fei-Fei, Deqing Sun, et al. Zeronvs: Zero-shot 360-degree view synthesis from a single real image. *arXiv preprint arXiv:2310.17994*, 2023. 3
- [79] Axel Sauer, Tero Karras, Samuli Laine, Andreas Geiger, and Timo Aila. Stylegan-t: Unlocking the power of gans for fast large-scale text-to-image synthesis. In *International Conference on Machine Learning (ICML)*, 2023. 2
- [80] Christoph Schuhmann, Richard Vencu, Romain Beaumont, Robert Kaczmarczyk, Clayton Mullis, Aarush Katta, Theo Coombes, Jenia Jitsev, and Aran Komatsuzaki. Laion-400m: Open dataset of clip-filtered 400 million image-text pairs. *arXiv preprint arXiv:2111.02114*, 2021. 2
- [81] Jing Shi, Wei Xiong, Zhe Lin, and Hyun Joon Jung. Instantbooth: Personalized text-to-image generation without test-time finetuning. *arXiv preprint arXiv:2304.03411*, 2023. 3
- [82] Yichun Shi, Peng Wang, Jianglong Ye, Mai Long, Kejie Li, and Xiao Yang. Mvdream: Multi-view diffusion for 3d generation. In *International Conference on Learning Representations (ICLR)*, 2024. 3
- [83] Jascha Sohl-Dickstein, Eric Weiss, Niru Maheswaranathan, and Surya Ganguli. Deep unsupervised learning using nonequilibrium thermodynamics. In *International Conference on Machine Learning (ICML)*, 2015. 2, 3
- [84] Chonghyuk Song, Gengshan Yang, Kangle Deng, Jun-Yan Zhu, and Deva Ramanan. Total-recon: Deformable scene reconstruction for embodied view synthesis. In *IEEE International Conference on Computer Vision (ICCV)*, 2023. 9, 11
- [85] Jiaming Song, Chenlin Meng, and Stefano Ermon. Denoising diffusion implicit models. In *International Conference on Learning Representations (ICLR)*, 2021. 2, 3
- [86] Matthew Tancik, Ben Mildenhall, Terrance Wang, Divi Schmidt, Pratul P Srinivasan, Jonathan T Barron, and Ren Ng. Learned initializations for optimizing coordinate-based neural representations. In *IEEE Conference on Computer Vision and Pattern Recognition (CVPR)*, 2021. 3
- [87] Matthew Tancik, Ethan Weber, Evonne Ng, Ruilong Li, Brent Yi, Terrance Wang, Alexander Kristoffersen, Jake Austin, Kamyar Salahi, Abhik Ahuja, et al. Nerfstudio: A modular framework for neural radiance field development. In *ACM SIGGRAPH 2023 Conference Proceedings*, 2023. 8, 17
- [88] Jiayang Tang, Jiawei Ren, Hang Zhou, Ziwei Liu, and Gang Zeng. Dreamgaussian: Generative gaussian splatting for efficient 3d content creation. *arXiv preprint arXiv:2309.16653*, 2023. 3
- [89] Yoad Tewel, Rinon Gal, Gal Chechik, and Yuval Atzmon. Key-locked rank one editing for text-to-image personalization. In *ACM SIGGRAPH 2023 Conference Proceedings*, 2023. 3
- [90] Dani Valevski, Danny Lumen, Yossi Matias, and Yaniv Leviathan. Face0: Instantaneously conditioning a text-to-image model on a face. In *SIGGRAPH Asia 2023 Conference Papers*, 2023. 3
- [91] Ashish Vaswani, Noam Shazeer, Niki Parmar, Jakob Uszkoreit, Llion Jones, Aidan N Gomez, Lukasz Kaiser, and Illia Polosukhin. Attention is all you need. In *Conference on Neural Information Processing Systems (NeurIPS)*, 2017. 4
- [92] Andrey Voynov, Qinghao Chu, Daniel Cohen-Or, and Kfir Aberman. $p+$: Extended textual conditioning in text-to-image generation. *arXiv preprint arXiv:2303.09522*, 2023. 3
- [93] Sheng-Yu Wang, Alexei A Efros, Jun-Yan Zhu, and Richard Zhang. Evaluating data attribution for text-to-image models. In *IEEE International Conference on Computer Vision (ICCV)*, 2023. 8
- [94] Yuxiang Wei, Yabo Zhang, Zhilong Ji, Jinfeng Bai, Lei Zhang, and Wangmeng Zuo. Elite: Encoding visual concepts into textual embeddings for customized text-to-image generation. In *IEEE International Conference on Computer Vision (ICCV)*, 2023. 3
- [95] Rundi Wu, Ben Mildenhall, Philipp Henzler, Keunhong Park, Ruiqi Gao, Daniel Watson, Pratul P Srinivasan, Dor Verbin, Jonathan T Barron, Ben Poole, et al. Reconfusion: 3d reconstruction with diffusion priors. *arXiv preprint arXiv:2312.02981*, 2023. 3
- [96] Shunyu Yao, Tzu Ming Hsu, Jun-Yan Zhu, Jiajun Wu, Antonio Torralba, Bill Freeman, and Josh Tenenbaum. 3d-aware scene manipulation via inverse graphics. In *Conference on Neural Information Processing Systems (NeurIPS)*, 2018. 3
- [97] Jianglong Ye, Naiyan Wang, and Xiaolong Wang. Feature-erf: Learning generalizable nerfs by distilling foundation models. In *IEEE International Conference on Computer Vision (ICCV)*, 2023. 4
- [98] Alex Yu, Vickie Ye, Matthew Tancik, and Angjoo Kanazawa. pixelnerf: Neural radiance fields from one or few images. In *IEEE Conference on Computer Vision and Pattern Recognition (CVPR)*, 2021. 3, 4
- [99] Jiahui Yu, Yuanzhong Xu, Jing Yu Koh, Thang Luong, Gunjan Baid, Zirui Wang, Vijay Vasudevan, Alexander Ku, Yinfei Yang, Burcu Karagol Ayan, et al. Scaling autoregressive models for content-rich text-to-image generation. In *International Conference on Machine Learning (ICML)*, 2022. 2

- [100] Jason Y Zhang, Deva Ramanan, and Shubham Tulsiani. Rel-pose: Predicting probabilistic relative rotation for single objects in the wild. In *European Conference on Computer Vision (ECCV)*, 2022. 8
- [101] Jason Y Zhang, Amy Lin, Moneish Kumar, Tzu-Hsuan Yang, Deva Ramanan, and Shubham Tulsiani. Cameras as rays: Sparse-view pose estimation via ray diffusion. In *International Conference on Learning Representations (ICLR)*, 2024. 8, 16
- [102] Lvmin Zhang and Maneesh Agrawala. Adding conditional control to text-to-image diffusion models. In *IEEE International Conference on Computer Vision (ICCV)*, 2023. 2
- [103] Yuxuan Zhang, Wenzheng Chen, Huan Ling, Jun Gao, Yinan Zhang, Antonio Torralba, and Sanja Fidler. Image gans meet differentiable rendering for inverse graphics and interpretable 3d neural rendering. In *International Conference on Learning Representations (ICLR)*, 2021. 3
- [104] Yuxin Zhang, Weiming Dong, Fan Tang, Nisha Huang, Haibin Huang, Chongyang Ma, Tong-Yee Lee, Oliver Deussen, and Changsheng Xu. Prospect: Prompt spectrum for attribute-aware personalization of diffusion models. *ACM Transactions on Graphics (TOG)*, 2023. 3
- [105] Xingyi Zhou, Rohit Girdhar, Armand Joulin, Philipp Krähenbühl, and Ishan Misra. Detecting twenty-thousand classes using image-level supervision. In *European Conference on Computer Vision (ECCV)*, 2022. 16
- [106] Zhizhuo Zhou and Shubham Tulsiani. Sparsefusion: Distilling view-conditioned diffusion for 3d reconstruction. In *IEEE Conference on Computer Vision and Pattern Recognition (CVPR)*, 2023. 3

Appendix

In Appendix A, we show more results and baseline comparisons. In Appendix B, we provide details regarding the evaluation and human preference study. Finally, in Appendix C, we describe all the implementation details of our method and baselines.

A. Results

More baselines. We add a comparison to SDEdit with the Stable Diffusion-XL model here, which we found to perform worse or on par with the Stable Diffusion-1.5 version of the model. Figure 10 shows the quantitative comparison.

Per category comparison. We show text-alignment and image-alignment scores of our method and baselines for each category in Figure 10 while varying the text guidance scale for each method from 5.0 to 10.0, except for LEDITS++ [8] which recommends varying the concept editing guidance scale from 10.0 to 15.0. For each guidance scale, we generate 288 images. Our method usually results in a higher CLIP score than the baselines, indicating better text alignment. For all categories, we show the linear fit curve over the different guidance scales, and our method lies at the Pareto-frontal compared to the baseline methods, either performing similarly or better.

Using predicted masks for background losses. In our main paper, we calculated the background losses (Eqn. 11) using ground truth masks from the dataset during training. We show in Table 4 that replacing these with predicted masks results in similar performance. We use Detic [105] with Segment Anything [44] to predict the object mask given the object category, such as car and teddy bear.

Varying number of views. In all our experiments, we use ~ 50 multi-view images and their ground truth poses for training. Here, we vary the number of multi-view images to 35 and 20, respectively, and show its results in Table 4. As the number of views decreases, text alignment remains similar, but the accuracy of camera pose and image alignment gradually decreases. Example generations and their comparison to our main method are shown in Figure 13.

Qualitative comparison. We show more qualitative comparisons between our method and baselines in Figure 15. Figure 16 shows more samples from varying camera poses for our method.

Comparison to LoRA. We compare our method to the customization method LoRA [32, 76] on the text and image alignment metrics here. The CLIP and DINO scores for LoRA are 0.275 and 0.468, respectively. In comparison, our CLIP and DINO scores are 0.253 and 0.481, respectively. Though the CLIP score is marginally lower, our method performs better in preserving the target concept while allowing additional camera pose control for the custom object.

Method	Text Alignment	Image Alignment	Camera-pose Accuracy	
	CLIPScore \uparrow	DINO-v2 \uparrow	Angular error \downarrow	Camera center error \downarrow
Ours	0.248	0.471	14.19	0.080
w/ predicted mask	0.246	0.475	13.80	0.086
w/ 35 views	0.250	0.439	18.09	0.108
w/ 20 views	0.254	0.448	18.96	0.108

Table 4. **Results with predicted masks and variable views.** Our method works similarly even when using predicted masks instead of ground truth masks for mask-based losses. When varying the number of views, the performance gradually drops w.r.t. camera pose accuracy and image alignment.

B. Evaluation.

Evaluation text prompts. As mentioned in the main paper, we used ChatGPT to generate text prompts for evaluating our method and baselines. Table 5 lists all of the prompts. An example instruction given to ChatGPT to generate prompts for the motorcycle category is: “Provide 16 diverse captions for plausible naturally occurring images of a motorcycle. Only follow one of the options given below while generating the captions. Thus, four captions per option. Each caption should have a simple sentence structure. (1) change the background scene of the motorcycle, (2) insert a new object in the scene with the motorcycle (3) change the type of the motorcycle (4) change the color of the motorcycle”.

Evaluation camera pose. Figure 11 shows sample training and validation camera poses for the car object. To measure the camera pose accuracy, we randomly select 6 validation camera poses (Figure 11, 2nd column) and generate images using one of the 16 text prompts. We then use RayDiffusion [101] to predict the camera pose from the 6 generated images and calculate its error with the target camera pose. The validation camera poses are such that the principal axis of the camera points towards the object. For text- and image-alignment metrics, we use the perturbed validation camera poses (Figure 11, 3rd column).

Human preference study. We perform a pairwise comparison of our method with each baseline. To measure text alignment, we show the input text prompt and the two images generated by ours and the baseline method, respectively, and ask: “Which image is more consistent with the following text?” For the image alignment, we show 3-4 target images at the top and ask: “Which of the below images is more consistent with the shown target object?” To measure photorealism, we only show the two generated images with the question: “Which of the below images is more photorealistic?”

DINO image alignment metrics. We use DINOv2 [59] as the pretrained model to measure image alignment. For each generated image, we measure its mean similarity to all the training images of the target concept. We crop the object region in the training images using masks to measure the similarity only with the target concept.

C. Implementation Details

C.1. Our Method

We fine-tune a pretrained Stable Diffusion-XL 32-bit floating point model with a batch size of 4. We update the new parameters with a learning rate of 1×10^{-4} . During training, we bias the sampling of time towards later time steps [56] since pose information is more crucial in the early stages of denoising. Training is done for 1600 iterations, which takes ~ 45 minutes on 4 A100-GPUs with 40GB VRAM. At each training step, we sample 5 views (maximum possible in GPU memory) equidistant from each other and use the first as the target viewpoint and the others as references. We crop the reference images tightly around the object bounding box and modify the camera intrinsics accordingly. We modify 12 transformer layers with pose-conditioning out of a total of 70 transformer layers in Stable Diffusion-XL, with 4 in the encoder, 3 in the middle, and 5 in the decoder blocks of the U-Net. Further, in a particular encoder or decoder block, we use the density predicted by previous FeatureNeRF blocks to importance sample the points along the ray for the next FeatureNeRF block 90% of the times. This improves the performance on concepts with thin structures like chairs. For rendering, we sample 24 points along the ray. The training hyperparameters, λ_{rgb} , λ_s , λ_{bg} are set to 5, 10, and 10 for all experiments.

During inference, we use an image guidance scale of 3.5 and a text guidance scale of 7.5 in Eqn. 13. All images for evaluation are generated with 50 sampling steps using the default Euler scheduler [35]. With these settings, the wallclock runtime to generate one image given 8 reference views is 10 seconds. We cache the reference view features for each customized model. For comparison, it takes 6 seconds to generate an image given no reference views.

C.2. Baselines

For 2D image editing methods, we first render the image given the target camera pose using a trained NeRF model [87]. To remove floater artifacts outside of the object mask in the rendered image, we run a pre-processing step using the SDEdit Stable Diffusion-XL denoising ensemble [64] with negative prompts “blurry, blur”. The inpainted image is then passed to the 2D image editing method as the input. For each baseline, we calculate metrics at 5 different guidance scales and keep the remaining hyperparameters the same across all object categories as much as possible.

SDEdit [52]. This uses the forward process to create a noisy image at some intermediate timestep and runs the backward denoising process with the new text prompt. For the optimal strength value, we ran a grid search from 0.5 to 0.8. We report our evaluation metrics on the best-performing strength of 0.5 (highest average text alignment to image alignment ratio). We run all inference in float16. For SDEdit

with Stable Diffusion-1.5, we use the recommended PNDM sampler [48] and set the number of inference steps to 50. With a strength of 0.5, the number of denoising steps run is 25 and takes 1 second. In the case of Stable Diffusion-XL, we apply the base model and refiner model as an ensemble of expert denoisers [64]. We run the base model with the default Euler scheduler [35] for 15 steps at strength 0.5 and the refiner for 5 more steps. With these settings, the wallclock runtime to generate one image is 5 seconds.

LEDITS++ [8]. This is a more recent method that proposes a new inversion technique to embed the image in latent space. It then constructs semantically grounded masks from the U-Net’s cross-attention layers and noise estimates to constrain the edit regions corresponding to the new text prompt. The user must adjust the LEDITS++ hyperparameter values according to whether they wish to modify large or small regions of the image, e.g., background changes vs. object appearance edits. To find the best hyperparameters, we refer to the recommended values provided in the official implementation. Thus, for prompts that edit the object’s appearance, we keep the target prompt guidance scale at 8, the edited concept’s threshold at 0.9, the default number of inference steps at 50, and the proportion of initial denoising steps skipped to 0.25. For prompts that change the background significantly, we additionally change the target prompt from the original image’s BLIP caption [46] to the background-changing prompt. For example, the edit in Figure 13 is achieved in LEDITS++ by changing the target prompt from “A teddy bear sitting on a table in a living room” to “A teddybear on the sand at the beach”. On the other hand, to edit the color of the teddy bear to gray using LEDITS++, the target prompt would still be “A teddy bear sitting on a table in a living room” but the concept “A gray teddybear” would be added to guided the generated image in that direction.

InstructPix2Pix [9]. This image-editing technique trains a model to follow editing instructions and can edit a new input image in a feedforward manner. We use the official model released with the paper based on Stable Diffusion-1.5, set the image guidance scale to the suggested value of 1.5, and use the default Euler scheduler with 50 inference steps.

ViCA-NeRF [20]. This is a 3D editing method that provides improved multiview consistency and training speed compared to Instruct-NeRF2NeRF [27]. First, the editing stage edits key views from the set of multiview images using InstructPix2Pix, reprojects the editing results to other views using the camera pose and depth information, and blends the edits in the latent diffusion model’s feature space. Second, the NeRF training stage uses the edited multiview images to optimize the unedited NeRF and produce a 3D-edited NeRF. We use the official implementation’s hyperparameters of text guidance scale 7.5 and image guidance scale 1.5. For concepts from the NAVI dataset, we select images from a single scene. For our method, we use images from multiple

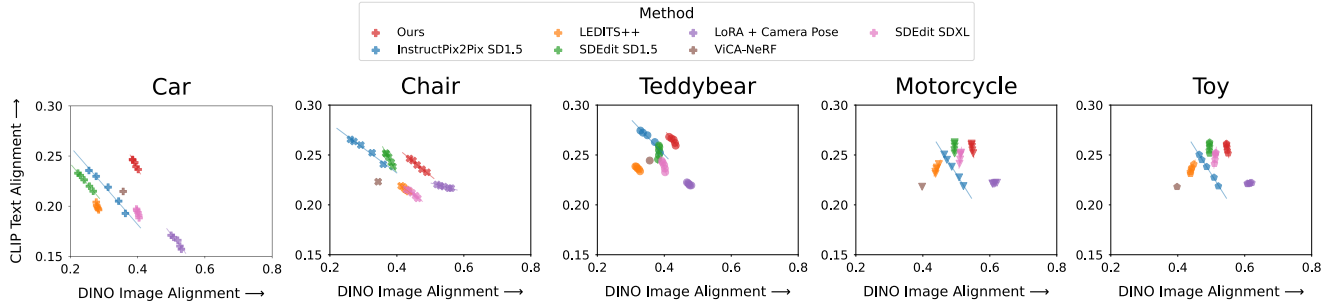


Figure 10. **CLIP vs. DINO scores, separated by object category.** For each category, our method achieves higher or the same text alignment compared to baselines while having on-par image alignment.)

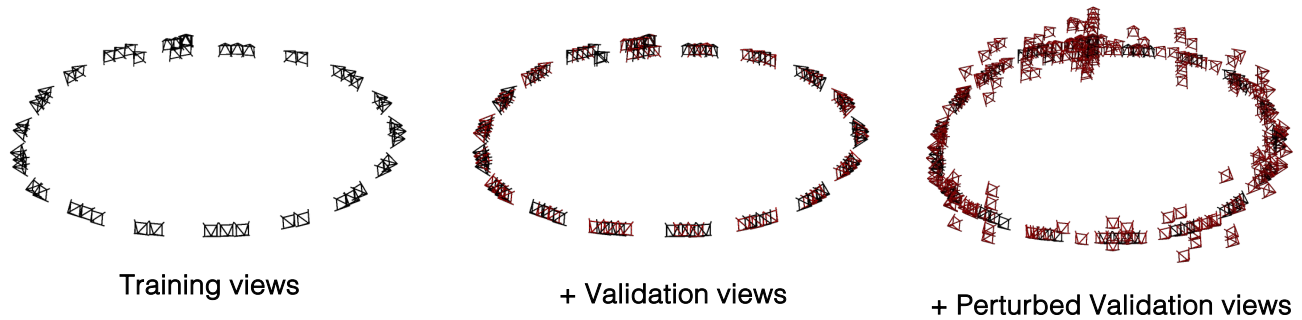


Figure 11. **Sample training and validation (+perturbed) views.** We show sample training and validation views that we use in our method. For quantitative evaluation, we perturb the location and focal length of the validation camera poses to create the final set of evaluation target camera poses.

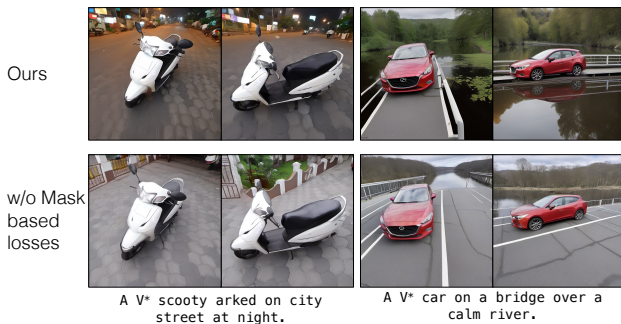


Figure 12. **Role of mask-based loss in FeatureNeRF.** Not having silhouette and background losses results in the model overfitting to the background features of the training image, e.g., the trees in the background.

scenes since we only model the foreground object.

LoRA [32]. This is a 2D customization method that trains low-rank adapters in linear layers of the diffusion model U-Net when fine-tuning on the new custom concept. We fine-tune Stable Diffusion-XL using the LoRA fine-tuning technique with rank 64 adapters added to all the linear layers in the attention blocks. We use the recommended learning rate of 1×10^{-4} with batch-size 16 and train for 1000 itera-

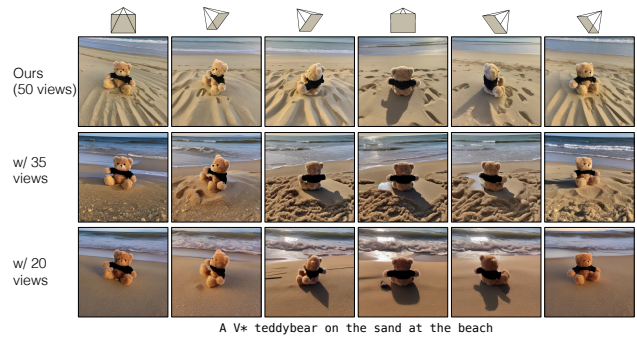


Figure 13. **Number of training views.** As we decrease the number of training views, some target camera poses are not respected in the output generations, specifically back-facing viewpoints. We observe that the model has a bias towards generating front-facing objects.

tions. We sample the regularization images as in our method 25% of the times. For training, we use the text prompt photo of a V^* {category}, where V^* is a fixed token.

LoRA + Camera pose. We modify the LoRA customization method to include the camera pose condition and text prompt. To achieve this, in every cross-attention layer, we concatenate the flattened camera projection matrix with the

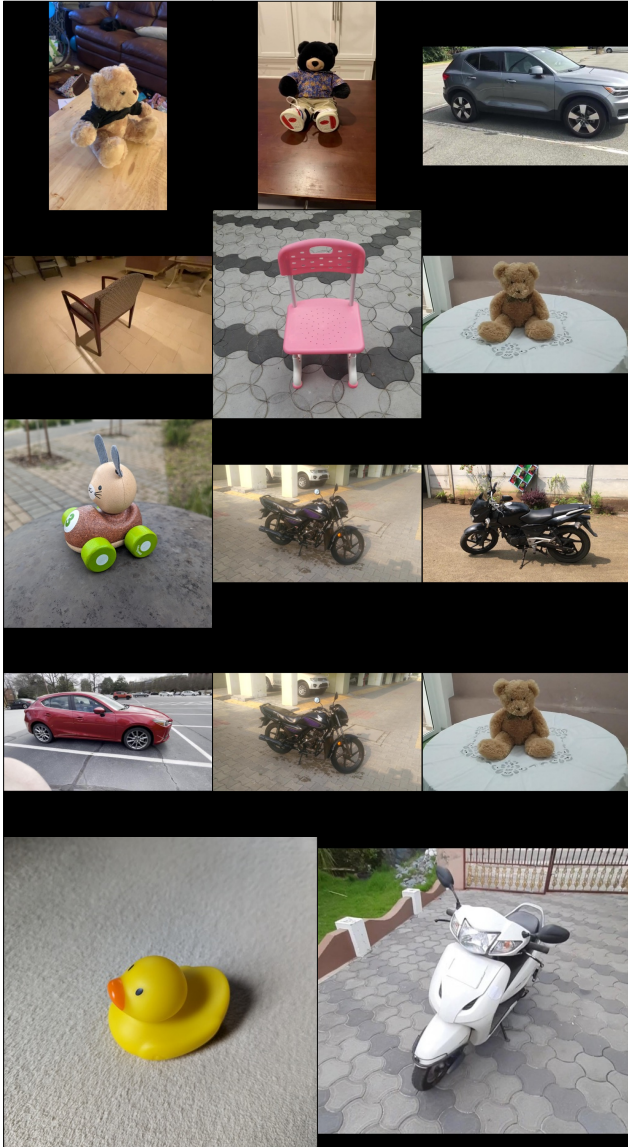


Figure 14. **Target concepts.** Sample images from the 14 target concepts used as the dataset for evaluating our method.

text transformer output along the feature dimension and use a one-layer MLP to project it back to the original dimension. The one-layer MLP is trained along with LoRA adapter modules, with all other hyperparameters kept the same as the above LoRA baseline. To match our method, we also biased the sampling of time towards later time steps. Like ours, the reconstruction loss is only applied in the masked region. We train the model for a total of 2000 iterations.

Object Category	Evaluation Prompt
Car	A car parked by a snowy mountain range.
	A car on a bridge over a calm river.
	A car in front of an old, brick train station.
	A car beside a field of blooming sunflowers.
	A car with a bike rack on top.
	A car next to a picnic table in a park.
	A car with a guitar leaning against it.
	A car with a kayak mounted on the roof.
	A minivan car outside a school, during pickup time.
	A convertible car near a coastal boardwalk.
	A jeep car on a rugged dirt road.
	A volkswagon beetle car in front of a luxury hotel.
	A red car in a mall parking lot.
	A yellow car at a gas station.
A green car in a driveway, next to a house.	
A black car in a busy city street.	
Chair	A chair on a balcony overlooking the city skyline.
	A chair in a garden surrounded by flowers.
	A chair on a beach.
	A chair in a library next to a bookshelf.
	A chair with a plush toy sitting on it.
	A chair beside a guitar on a stand.
	A chair next to a potted plant.
	A chair with a colorful cushion on it.
	A rocking chair on a porch.
	An office chair in a home study.
	A folding chair at a camping site.
	A high chair in a kitchen.
	A red chair in a white room.
	A black chair in a classroom.
A green chair in a café.	
A yellow chair in a playroom.	
Teddybear	A teddybear on a park bench under trees.
	A teddybear at a window with raindrops outside.
	A teddybear on the sand at the beach.
	A teddybear on a cozy armchair by a fireplace.
	A teddybear with a stack of children's books on the side.
	A teddybear next to a birthday cake with candles.
	A teddybear with a small toy car.
	A teddybear holding a heart-shaped balloon.
	A teddybear in a pink barbie costume.
	A large teddybear in a batman costume.
	A teddybear dressed as a construction worker.
	A teddybear in a superhero costume.
	A pink teddybear on a shelf.
	A brown teddybear on a blanket.
A white teddybear.	
A gray teddybear.	
Motorcycle	A motorcycle parked on a city street at night.
	A motorcycle beside a calm lake.
	A motorcycle on a mountain road with a scenic view.
	A motorcycle in front of a graffiti-covered urban wall.
	A motorcycle with a guitar strapped to the back.
	A motorcycle next to a camping tent.
	A golden retriever riding motorcycle.
	A cat riding motorcycle.
	A cruiser motorcycle in a parking lot.
	A scooter like motorcycle.
	A vintage style motorcycle.
	A dirt bike motorcycle on a trail in the woods.
	A red motorcycle in a garage.
	A green motorcycle.
A blue motorcycle.	
A silver motorcycle.	
Toy	Toy on a sandy beach, with waves crashing in the background
	A toy sitting in a grassy field, surrounded by wildflowers.
	A toy on a rocky mountain top, overlooking the valley below.
	A toy in a dense jungle.
	A toy with a tiny book placed beside it on a wooden table.
	A toy floating next to a colorful beach ball in a bathtub.
	A toy with a small globe resting next to it.
	A toy and an umbrella in a cozy living room.
	A plush toy on a sunny windowsill.
	A wooden toy.
	An origami of toy.
	A clay figurine of toy.
	A bright red toy.
	A deep blue toy on a bed.
A vivid green toy.	
A neon pink toy.	

Table 5. **Evaluation prompts.** Here, we list the final prompts that were used for evaluation for the car, chair, teddy bear, motorcycle, and toy categories.

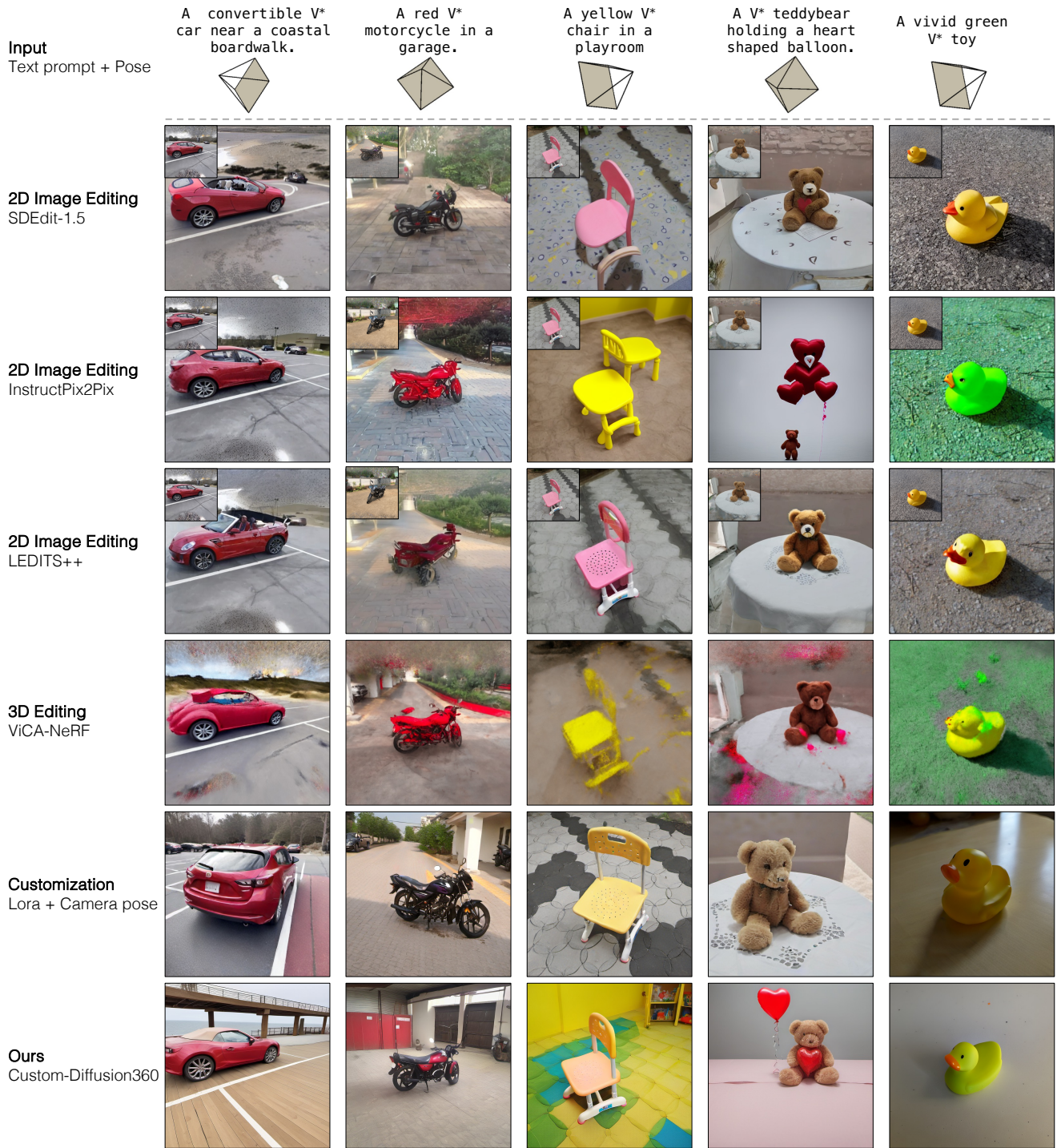


Figure 15. Additional qualitative comparison of our method with baselines, given various prompts and target pose conditions.

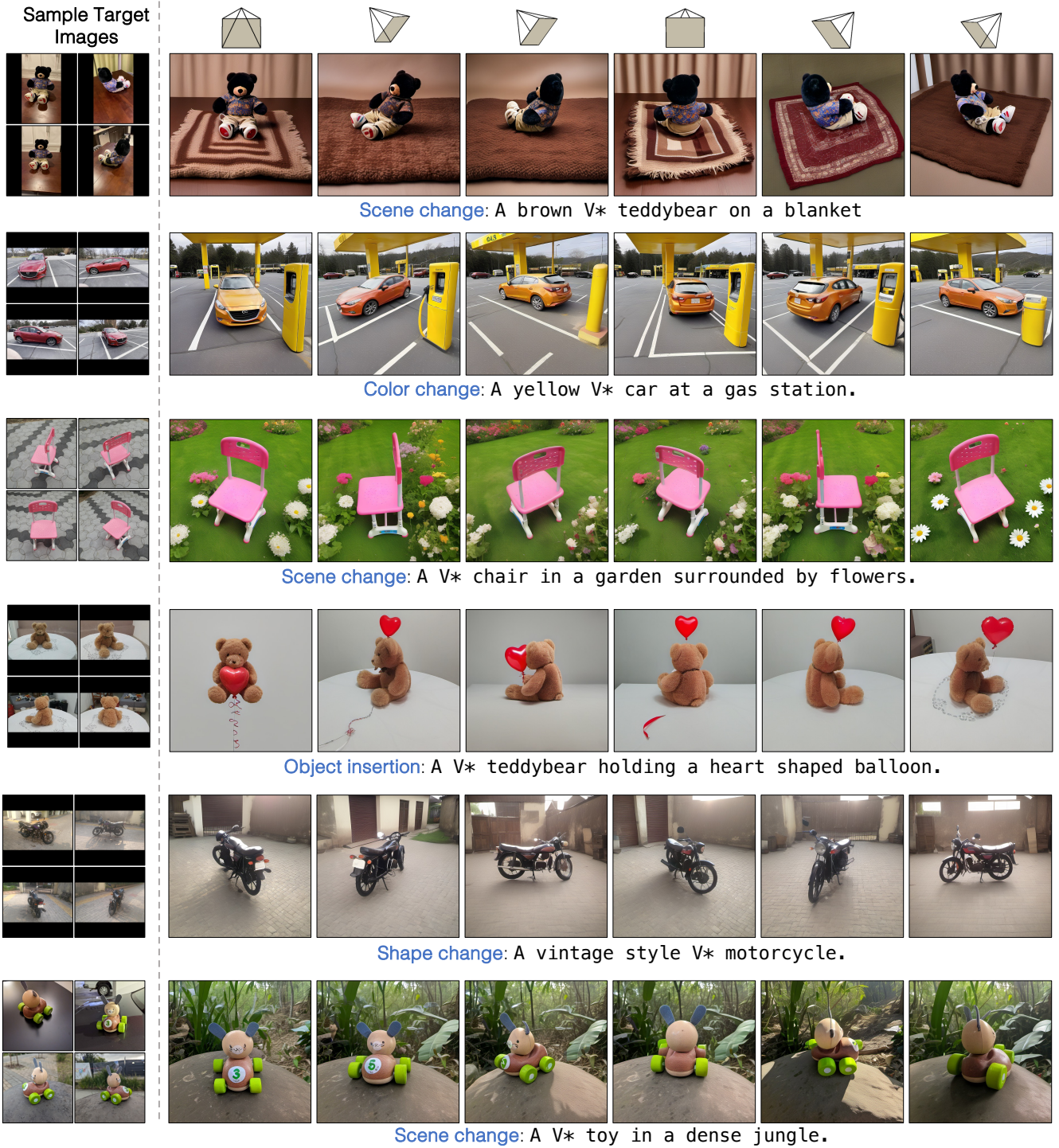


Figure 16. Additional qualitative samples of our method while varying the camera pose condition for the custom object.